

---

# Subgroup Generalization and Fairness of Graph Neural Networks

---

Jiaqi Ma<sup>\*†</sup>  
jiaqima@umich.edu

Junwei Deng<sup>\*†</sup>  
junweid@umich.edu

Qiaozhu Mei<sup>\*‡</sup>  
qmei@umich.edu

## Abstract

Despite enormous successful applications of graph neural networks (GNNs), theoretical understanding of their generalization ability, especially for node-level tasks where data are not independent and identically-distributed (IID), has been sparse. The theoretical investigation of the generalization performance is beneficial for understanding fundamental issues (such as fairness) of GNN models and designing better learning methods. In this paper, we present a novel PAC-Bayesian analysis for GNNs under a non-IID semi-supervised learning setup. Moreover, we analyze the generalization performances on different subgroups of unlabeled nodes, which allows us to further study an accuracy-(dis)parity-style (un)fairness of GNNs from a theoretical perspective. Under reasonable assumptions, we demonstrate that the distance between a test subgroup and the training set can be a key factor affecting the GNN performance on that subgroup, which calls special attention to the training node selection for fair learning. Experiments across multiple GNN models and datasets support our theoretical results<sup>4</sup>.

## 1 Introduction

Graph Neural Networks (GNNs) [13, 35, 20] are a family of machine learning models that can be used to model non-Euclidean data as well as inter-related samples in a flexible way. In recent years, there have been enormous successful applications of GNNs in various areas, such as drug discovery [18], computer vision [29], transportation forecasting [49], recommender systems [48], etc. Depending on the type of prediction target, the application tasks can be roughly categorized into node-level, edge-level, subgraph-level, and graph-level tasks [46].

In contrast to the marked empirical success, theoretical understanding of the generalization ability of GNNs has been rather limited. Among the existing literature, some studies [9, 11, 25] focus on the analysis of graph-level tasks where each sample is an entire graph and the samples of graphs are IID. A very limited number of studies [36, 42] explore GNN generalization for node-level tasks but they assume the nodes (and their associated neighborhoods) are IID samples, which does not align with the commonly seen graph-based semi-supervised learning setups. Baranwal et al. [3] investigate GNN generalization without IID assumptions but under a specific data generating mechanism.

In this work, our first contribution is to provide a novel PAC-Bayesian analysis for the generalization ability of GNNs on node-level tasks with non-IID assumptions. In particular, we assume the node features are fixed and the node labels are independently sampled from distributions conditioned on the node features. We also assume the training set and the test set can be chosen as arbitrary subsets of nodes on the graph. We first prove two general PAC-Bayesian generalization bounds (Theorem 1

---

<sup>\*</sup>School of Information, University of Michigan, Ann Arbor, Michigan, USA

<sup>†</sup>Equal contribution.

<sup>‡</sup>Department of EECS, University of Michigan, Ann Arbor, Michigan, USA

<sup>4</sup>Code available at <https://github.com/TheaperDeng/GNN-Generalization-Fairness>.

and Theorem 2) under this non-IID setup. Subsequently, we derive a generalization bound for GNN (Theorem 3) in terms of characteristics of the GNN models and the node features.

Notably, the generalization bound for GNN is influenced by the distance between the test nodes and the training nodes in terms of their aggregated node features. This suggests that, given a fixed training set, test nodes that are “far away” from all the training nodes may suffer from larger generalization errors. Based on this analysis, our second contribution is the discovering of a type of unfairness that arises from theoretically predictable accuracy disparity across some subgroups of test nodes. We further conduct an empirical study that investigates the prediction accuracy of four popular GNN models on different subgroups of test nodes. The results on multiple benchmark datasets indicate that there is indeed a significant disparity in test accuracy among these subgroups.

We summarize the contributions of this work as follows:

- (1) We establish a novel PAC-Bayesian analysis for graph-based semi-supervised learning with non-IID assumptions.
- (2) Under this setup, we derive a generalization bound for GNNs that can be applied to an arbitrary subgroup of test nodes.
- (3) As an implication of the generalization bound, we predict that there would be an unfairness of GNN predictions that arises from accuracy disparity across subgroups of test nodes.
- (4) We empirically verify the existence of accuracy disparity of popular GNN models on multiple benchmark datasets, as predicted by our theoretical analysis.

## 2 Related Work

### 2.1 Generalization of Graph Neural Networks

The majority of existing literature that aims to develop theoretical understandings of GNNs have focused on the expressive power of GNNs (see Sato [34] for a survey along this line), while the number of studies trying to understand the generalizability of GNNs is rather limited. Among them, some [9, 11, 25] focus on graph-level tasks, the analyses of which cannot be easily applied to node-level tasks. As far as we know, Scarselli et al. [36], Verma and Zhang [42], and Baranwal et al. [3] are the only existing studies investigating the generalization of GNNs on node-level tasks, even though node-level tasks are more common in reality. Scarselli et al. [36] present an upper bound of the VC-dimension of GNNs; Verma and Zhang [42] derive a stability-based generalization bound for a single-layer GCN [20] model. Yet, both Scarselli et al. [36] and Verma and Zhang [42] (implicitly) assume that the training nodes are IID samples from a certain distribution, which does not align with the common practice of node-level semi-supervised learning. Baranwal et al. [3] investigate the generalization of graph convolution under a specific data generating mechanism (i.e., the contextual stochastic block model [8]). Our work presents the first generalization analysis of GNNs for non-IID node-level tasks without strong assumptions on the data generating mechanism.

### 2.2 Fairness of Machine Learning on Graphs

The fairness issues of machine learning on graphs start to receive research attention recently. Following conventional machine learning fairness literature, the majority of previous work along this line [1, 5–7, 22, 32, 39, 50] concerns about fairness with respect to a given sensitive attribute, such as gender or race, which defines protected groups. In practice, the fairness issues of learning on graphs are much more complicated due to the asymmetric nature of the graph-structured data. However, only a few studies [19] investigate the unfairness caused by the graph structure without knowing a sensitive feature. Moreover, in a node-level semi-supervised learning task, the non-IID sampling of training nodes brings additional uncertainty to the fairness of the learned models. This work is the first to present a learning theoretic analysis under this setup, which in turn suggests how the graph structure and the selection of training nodes may influence the fairness of machine learning on graphs.

### 2.3 PAC-Bayesian Analysis

PAC-Bayesian analysis [27] has become one of the most powerful theoretical framework to analyze the generalization ability of machine learning models. We will briefly introduce the background in

Section 3.2, and refer the readers to a recent tutorial [14] for a systematic overview of PAC-Bayesian analysis. We note that Liao et al. [25] recently present a PAC-Bayesian generalization bound for GNNs on IID graph-level tasks. Both Liao et al. [25] and this work utilize results from Neyshabur et al. [30], a PAC-Bayesian analysis for ReLU-activated neural networks, in part of our proofs. Compared to Neyshabur et al. [30], the key contribution of Liao et al. [25] is the derivation of perturbation bounds of two types of GNN architectures; while the key contribution of this work is the novel analysis under the setup of non-IID node-level tasks. There is also an existing work of PAC-Bayesian analysis for transductive semi-supervised learning [4]. But it is different from our problem setup and, in particular, it cannot be used to analyze the generalization on subgroups.

### 3 Preliminaries

In this section, we first formulate the problem of node-level semi-supervised learning. We also provide a brief introduction of the PAC-Bayesian framework.

#### 3.1 The Problem Formulation and Notations

**Semi-supervised node classification.** Let  $G = (V, E) \in \mathcal{G}_N$  be an undirected graph, with  $V = \{1, 2, \dots, N\}$  being the set of  $N$  nodes and  $E \subseteq V \times V$  being the set of edges. And  $\mathcal{G}_N$  is the space of all undirected graphs with  $N$  nodes. The nodes are associated with node features  $X \in \mathbb{R}^{N \times D}$  and node labels  $y \in \{1, 2, \dots, K\}^N$ .

In this work, we focus on the transductive node classification setting [47], where the node features  $X$  and the graph  $G$  are observed prior to learning, and every quantity of interest in the analysis will be conditioned on  $X$  and  $G$ . Without loss of generality, we treat  $X$  and  $G$  as fixed throughout our analysis, and the randomness comes from the labels  $y$ . In particular, we assume that for each node  $i \in V$ , its label  $y_i$  is generated from an unknown conditional distribution  $\Pr(y_i | Z_i)$ , where  $Z = g(X, G)$  and  $g : \mathbb{R}^{N \times D} \times \mathcal{G}_N \rightarrow \mathbb{R}^{N \times D'}$  is an aggregation function that aggregates the features over (multi-hop) local neighborhoods<sup>5</sup>. We also assume that the node labels are generated independently conditional on their respective aggregated features  $Z_i$ 's.

Given a small set of the labeled nodes,  $V_0 \subseteq V$ , the task of node-level semi-supervised learning is to learn a classifier  $h : \mathbb{R}^{N \times D} \times \mathcal{G}_N \rightarrow \mathbb{R}^{N \times K}$  from a function family  $\mathcal{H}$  and perform it on the remaining unlabeled nodes. Given a classifier  $h$ , the classification for a node  $i$  is obtained by

$$\hat{y}_i = \operatorname{argmax}_{k \in \{1, \dots, K\}} h_i(X, G)[k],$$

where  $h_i(X, G)$  is the  $i$ -th row of  $h(X, G)$  and  $h_i(X, G)[k]$  refers to the  $k$ -th element of  $h_i(X, G)$ .

**Subgroups.** In Section 4, we will present an analysis of the GNN generalization performance on any subgroup of the set of unlabeled nodes,  $V \setminus V_0$ . Note that the analysis on any subgroup is a stronger result than that on the entire unlabeled set, as any set is a subset of itself. Later we will show that the analysis on subgroups (rather than on the entire set) further allows us to investigate the accuracy disparity across subgroups. We denote a collection of subgroups of interest as  $V_1, V_2, \dots, V_M \subseteq V \setminus V_0$ . In practice, a subgroup can be defined based on an attribute of the nodes (e.g., a gender group), certain graph-based properties, or an arbitrary partition of the nodes. We also define the size of each subgroup as  $N_m := |V_m|, m = 0, \dots, M$ .

**Margin loss on each subgroup.** Now we can define the *empirical* and *expected margin loss* of any classifier  $h \in \mathcal{H}$  on each subgroup  $V_m, m = 0, 1, \dots, M$ . Given a sample of observed node labels  $y_i$ 's, the empirical margin loss of  $h$  on  $V_m$  for a margin  $\gamma \geq 0$  is defined as

$$\hat{\mathcal{L}}_m^\gamma(h) := \frac{1}{N_m} \sum_{i \in V_m} \mathbb{1} \left[ h_i(X, G)[y_i] \leq \gamma + \max_{k \neq y_i} h_i(X, G)[k] \right], \quad (1)$$

where  $\mathbb{1}[\cdot]$  is the indicator function. The expected margin loss is the expectation of Eq. (1), i.e.,

$$\mathcal{L}_m^\gamma(h) := \mathbb{E}_{y_i \sim \Pr(y|Z_i), i \in V_m} \hat{\mathcal{L}}_m^\gamma(h). \quad (2)$$

<sup>5</sup>A simple example is  $g_i(X, G) = \frac{1}{|\mathcal{N}(i)|+1} \left( X_i + \sum_{j \in \mathcal{N}(i)} X_j \right)$ , where  $g_i(X, G)$  is the  $i$ -th row of  $g(X, G)$  and  $\mathcal{N}(i) := \{j \mid (i, j) \in E\}$  is the set of 1-hop neighbors of node  $i$ .

To simplify the notation, we define  $y^m := \{y_i\}_{i \in V_m}, \forall m = 0, \dots, M$ , so that Eq. (2) can be written as  $\mathcal{L}_m^\gamma(h) = \mathbb{E}_{y^m} \hat{\mathcal{L}}_m^\gamma(h)$ . We note that the classification *risk* and *empirical risk* of  $h$  on  $V_m$  are respectively equal to  $\mathcal{L}_m^0(h)$  and  $\hat{\mathcal{L}}_m^0(h)$ .

### 3.2 The PAC-Bayesian Framework

The PAC-Bayesian framework [27] is an approach to analyze the generalization ability of a stochastic predictor drawn from a distribution  $Q$  over the predictor family  $\mathcal{H}$  that is learned from the training data. For any stochastic classifier distribution  $Q$  and  $m = 0, \dots, M$ , slightly overloading the notation, we denote the empirical margin loss of  $Q$  on  $V_m$  as  $\hat{\mathcal{L}}_m^\gamma(Q)$ , and the corresponding expected margin loss as  $\mathcal{L}_m^\gamma(Q)$ . And they are given by

$$\hat{\mathcal{L}}_m^\gamma(Q) := \mathbb{E}_{h \sim Q} \hat{\mathcal{L}}_m^\gamma(h), \quad \mathcal{L}_m^\gamma(Q) := \mathbb{E}_{h \sim Q} \mathcal{L}_m^\gamma(h).$$

In general, a PAC-Bayesian analysis aims to bound the generalization gap between  $\mathcal{L}_m^\gamma(Q)$  and  $\hat{\mathcal{L}}_m^\gamma(Q)$ . The analysis is usually done by first proving that, for any “prior” distribution<sup>6</sup>  $P$  over  $\mathcal{H}$  that is independent of the training data, the generalization gap can be controlled by the discrepancy between  $P$  and  $Q$ ; the analysis is then followed by careful choices of  $P$  to get concrete upper bounds of the generalization gap. While the PAC-Bayesian framework is built on top of stochastic predictors, there exist standard techniques [23] that can be used to derive generalization bounds for deterministic predictors from PAC-Bayesian bounds.

Finally, we denote the *Kullback-Leibler (KL) divergence* as  $D_{\text{KL}}(Q \| P) := \int \ln \frac{dQ}{dP} dQ$ , which will be used in the following analysis.

## 4 The Generalization Bound and Its Implications for Fairness

As we mentioned in Section 2.3, existing PAC-Bayesian analyses cannot be directly applied to the non-IID semi-supervised learning setup where we care about the generalization (and its disparity) across different subgroups of the unlabeled samples. In this section, we first present general PAC-Bayesian theorems for subgroup generalization under our problem setup; then we derive a generalization bound for GNNs and discuss fairness implications of the bound.

### 4.1 General PAC-Bayesian Theorems for Subgroup Generalization

**Stochastic classifier bound.** We first present the general PAC-Bayesian theorem (Theorem 1) for subgroup generalization of stochastic classifiers. The generalization bound depends on a notion of *expected loss discrepancy* between two subgroups as defined below.

**Definition 1** (Expected Loss Discrepancy). *Given a distribution  $P$  over  $\mathcal{H}$ , for any  $\lambda > 0$  and  $\gamma \geq 0$ , for any two subgroups  $V_m$  and  $V_{m'}$  ( $0 \leq m, m' \leq M$ ), define the expected loss discrepancy between  $V_m$  and  $V_{m'}$  with respect to  $(P, \gamma, \lambda)$  as*

$$D_{m,m'}^\gamma(P; \lambda) := \ln \mathbb{E}_{h \sim P} e^{\lambda(\mathcal{L}_m^{\gamma/2}(h) - \mathcal{L}_{m'}^\gamma(h))},$$

where  $\mathcal{L}_m^{\gamma/2}(h)$  and  $\mathcal{L}_{m'}^\gamma(h)$  follow the definition of Eq. (2).

Intuitively,  $D_{m,m'}^\gamma(P; \lambda)$  captures the difference of the expected loss between  $V_m$  and  $V_{m'}$  in an average sense (over  $P$ ). Note that  $D_{m,m'}^\gamma(P; \lambda)$  is asymmetric in terms of  $V_m$  and  $V_{m'}$ , and can be negative if the loss on  $V_m$  is mostly smaller than that on  $V_{m'}$ .

For stochastic classifiers, we have the following Theorem 1. Proof can be found in Appendix A.1.

**Theorem 1** (Subgroup Generalization of Stochastic Classifiers). *For any  $0 < m \leq M$ , for any  $\lambda > 0$  and  $\gamma \geq 0$ , for any “prior” distribution  $P$  on  $\mathcal{H}$  that is independent of the training data on  $V_0$ , with*

<sup>6</sup>The distribution is called “prior” in the sense that it doesn’t depend on training data. “Prior” and “posterior” in PAC-Bayesian are different with those in conventional Bayesian statistics. See Guedj [14] for details.

probability at least  $1 - \delta$  over the sample of  $y^0$ , for any  $Q$  on  $\mathcal{H}$ , we have<sup>7</sup>

$$\mathcal{L}_m^{\gamma/2}(Q) \leq \widehat{\mathcal{L}}_0^\gamma(Q) + \frac{1}{\lambda} \left( D_{\text{KL}}(Q\|P) + \ln \frac{1}{\delta} + \frac{\lambda^2}{4N_0} + D_{m,0}^\gamma(P; \lambda) \right). \quad (3)$$

Theorem 1 can be viewed as an adaptation of a result by Alquier et al. [2] from the IID supervised setting to our non-IID semi-supervised setting. The terms  $D_{\text{KL}}(Q\|P)$ ,  $\ln \frac{2}{\delta}$ , and  $\frac{\lambda^2}{4N_0}$  are commonly seen in PAC-Bayesian analysis for IID supervised setting. In particular, when setting  $\lambda = \Theta(\sqrt{N_0})$ ,  $\frac{1}{\lambda} \left( \ln \frac{2}{\delta} + \frac{\lambda^2}{4N_0} \right)$  vanishes as the training size  $N_0$  grows. The divergence between  $Q$  and  $P$ ,  $D_{\text{KL}}(Q\|P)$ , is usually considered as a measurement of the model complexity [14]. And there will be a trade-off between the training loss,  $\widehat{\mathcal{L}}_0^\gamma(Q)$ , and the complexity (how far can the learned “posterior”  $Q$  go from the “prior”  $P$ ).

Uniquely for the non-IID semi-supervised setting, there is an extra term  $D_{m,0}^\gamma(P; \lambda)$ , which is the expected loss discrepancy between the target test subgroup  $V_m$  and the training set  $V_0$ . Note that this quantity is independent of the training labels  $y^0$ . Not surprisingly, it is difficult to give generalization guarantees if the expected loss on  $V_m$  is much larger than that on  $V_0$  for any stochastic classifier  $P$  independent of training data. We have to make some assumptions about the relationship between  $V_m$  and  $V_0$  to obtain a meaningful bound on  $\frac{1}{\lambda} D_{m,0}^\gamma(P; \lambda)$ , which we will discuss in details in Section 4.2.

**Deterministic classifier bound.** Utilizing standard techniques in PAC-Bayesian analysis [23, 27, 30], we can convert the bound for stochastic classifiers in Theorem 1 to a bound for deterministic classifiers as stated in Theorem 2 below (see Appendix A.2 for the proof).

**Theorem 2** (Subgroup Generalization of Deterministic Classifiers). *Let  $\tilde{h}$  be any classifier in  $\mathcal{H}$ . For any  $0 < m \leq M$ , for any  $\lambda > 0$  and  $\gamma \geq 0$ , for any “prior” distribution  $P$  on  $\mathcal{H}$  that is independent of the training data on  $V_0$ , with probability at least  $1 - \delta$  over the sample of  $y^0$ , for any  $Q$  on  $\mathcal{H}$  such that  $\Pr_{h \sim Q} \left( \max_{i \in V_0 \cup V_m} \|h_i(X, G) - \tilde{h}_i(X, G)\|_\infty < \frac{\gamma}{8} \right) > \frac{1}{2}$ , we have*

$$\mathcal{L}_m^0(\tilde{h}) \leq \widehat{\mathcal{L}}_0^\gamma(\tilde{h}) + \frac{1}{\lambda} \left( 2(D_{\text{KL}}(Q\|P) + 1) + \ln \frac{1}{\delta} + \frac{\lambda^2}{4N_0} + D_{m,0}^{\gamma/2}(P; \lambda) \right). \quad (4)$$

Theorem 1 and 2 are not specific to GNNs and hold for any (respectively stochastic and deterministic) classifier under the semi-supervised setup. In Section 4.2, we will apply Theorem 2 to obtain a subgroup generalization bound that explicitly depends on the characteristics of GNNs and the data.

## 4.2 Subgroup Generalization Bound for Graph Neural Networks

**The GNN model.** We consider GNNs where the node feature aggregation step and the prediction step are separate. In particular, we assume the GNN classifier takes the form of  $h_i(X, G) = f(g_i(X, G); W_1, W_2, \dots, W_L)$ , where  $g$  is an aggregation function as we described in Section 3.1 and  $f$  is a ReLU-activated  $L$ -layer Multi-Layer Perceptron (MLP) with  $W_1, \dots, W_L$  as parameters for each layer<sup>8</sup>. Denote the largest width of all the hidden layers as  $b$ .

**Remark 1.** *There is a technical restriction on the possible choice of the aggregation function  $g$ . For the following derivation of the generalization bound (6) to be valid, we need the condition that the node labels  $y_i$ ’s are independent conditional on their aggregated features  $g_i(X, G)$ ’s, as introduced in the problem formulation in Section 3.1. However, we also note that this condition tends to hold when the aggregated features  $g_i(X, G)$ ’s contain rich information about the labels.*

**Upper-bounding  $D_{m,0}^\gamma(P; \lambda)$ .** To derive the generalization guarantee, we need to upper-bound the expected loss discrepancy  $D_{m,0}^\gamma(P; \lambda)$ . It turns out that we have to make some assumptions on the data in order to get a meaningful upper bound.

So far we have not had any restrictions on the conditional label distributions  $\Pr(y_i = k \mid g_i(X, G))$ . If the label distributions on  $V \setminus V_0$  can be arbitrarily different from those on  $V_0$ , the generalization

<sup>7</sup>Theorem 1 also holds when we substitute  $\mathcal{L}_m^{\gamma/2}(h)$  and  $\mathcal{L}_m^{\gamma/2}(Q)$  as  $\mathcal{L}_m^\gamma(h)$  and  $\mathcal{L}_m^\gamma(Q)$  respectively. But we state Theorem 1 in this form to ease the presentation of the later analysis.

<sup>8</sup>SGC [45] and APPNP [21] are special cases of GNNs in this form.

can be arbitrarily poor. We therefore assume that the label distributions conditional on aggregated features are smooth (Assumption 1).

**Assumption 1** (Smoothness of Data Distribution). *Assume there exist  $c$ -Lipschitz continuous functions  $\eta_1, \eta_2, \dots, \eta_K : \mathbb{R}^{D'} \rightarrow [0, 1]$ , such that, for any node  $i \in V$ ,*

$$\Pr(y_i = k \mid g_i(X, G)) = \eta_k(g_i(X, G)), \forall k = 1, \dots, K.$$

We also need to characterize the relationship between a target test subgroup  $V_m$  and the training set  $V_0$ . For this purpose, we define the distance from  $V_m$  to  $V_0$  and the concept of *near set* below.

**Definition 2** (Distance To Training Set and Near Set). *For each  $0 < m \leq M$ , define the distance from the subgroup  $V_m$  to the training set  $V_0$  as*

$$\epsilon_m := \max_{j \in V_m} \min_{i \in V_0} \|g_i(X, G) - g_j(X, G)\|_2.$$

*Further, for each  $i \in V_0$ , define the near set of  $i$  with respect to  $V_m$  as*

$$V_m^{(i)} := \{j \in V_m \mid \|g_i(X, G) - g_j(X, G)\|_2 \leq \epsilon_m\}.$$

*Clearly,*

$$V_m = \cup_{i \in V_0} V_m^{(i)}.$$

Then, with the Assumption 2 and 3 below, we can bound the expected loss discrepancy  $D_{m,0}^\gamma(P; \lambda)$  with the following Lemma 1 (see the proof in Appendix A.3).

**Assumption 2** (Equal-Sized and Disjoint Near Sets). *For any  $0 < m \leq M$ , assume the near sets of each  $i \in V_0$  with respect to  $V_m$  are disjoint and have the same size  $s_m \in \mathbb{N}^+$ .*

**Assumption 3** (Concentrated Expected Loss Difference). *Let  $P$  be a distribution on  $\mathcal{H}$ , defined by sampling the vectorized MLP parameters from  $\mathcal{N}(0, \sigma^2 I)$  for some  $\sigma^2 \leq \frac{(\gamma/8\epsilon_m)^{2/L}}{2b(\lambda N_0^{-\alpha} + \ln 2bL)}$ . For any  $L$ -layer GNN classifier  $h \in \mathcal{H}$  with model parameters  $W_1^h, \dots, W_L^h$ , define  $T_h := \max_{l=1, \dots, L} \|W_l^h\|_2$ . Assume that there exists some  $0 < \alpha < \frac{1}{4}$  satisfying*

$$\Pr_{h \sim P} \left( \mathcal{L}_m^{\gamma/4}(h) - \mathcal{L}_0^{\gamma/2}(h) > N_0^{-\alpha} + cK\epsilon_m \mid T_h^L \epsilon_m > \frac{\gamma}{8} \right) \leq e^{-N_0^{2\alpha}}.$$

**Lemma 1** (Bound for  $D_{m,0}^\gamma(P; \lambda)$ ). *Under Assumptions 1, 2 and 3, for any  $0 < m \leq M$ , any  $0 < \lambda \leq N_0^{2\alpha}$  and  $\gamma \geq 0$ , assume the “prior”  $P$  on  $\mathcal{H}$  is defined by sampling the vectorized MLP parameters from  $\mathcal{N}(0, \sigma^2 I)$  for some  $\sigma^2 \leq \frac{(\gamma/8\epsilon_m)^{2/L}}{2b(\lambda N_0^{-\alpha} + \ln 2bL)}$ . We have*

$$D_{m,0}^{\gamma/2}(P; \lambda) \leq \ln 3 + \lambda cK\epsilon_m. \quad (5)$$

Intuitively, what we need to bound  $D_{m,0}^\gamma(P; \lambda)$  is that the training set  $V_0$  is “representative” for  $V_m$ . This is reasonable in practice as it is natural to select the training samples according to the distribution of the population. Specifically, Assumption 2 assumes that  $V_m$  can be split into equal-sized partitions indexed by the training samples. The elements of each partition  $V_m^{(i)}$  are close to the corresponding training sample  $i$  but not so close to training samples other than  $i$ . This assumption is stronger than needed to obtain a meaningful bound on  $D_{m,0}^\gamma(P; \lambda)$ , and we can relax it by only assuming that most samples in  $V_m$  have proportional “close representatives” in  $V_0$ . But we keep Assumption 2 in this work, as it is intuitively clear and significantly eases the analysis and notations. Assumption 3 essentially assumes that the expected margin loss on  $V_m$  is not much larger than that on  $V_0$  when the number of samples becomes large. We first note that this assumption becomes trivially true in the degenerate case that all samples in  $V_m$  and  $V_0$  are IID. In this case,  $\mathcal{L}_m^{\gamma/4}(h) = \mathcal{L}_0^{\gamma/4}(h) < \mathcal{L}_0^{\gamma/2}(h) \leq 0$  for any classifier  $h$ . In Appendix A.5, we further provide a simple non-IID example where Assumption 3 holds.

The bound (5) suggests that the closer between  $V_m$  and  $V_0$  (smaller  $\epsilon_m$ ), the smaller the expected loss discrepancy.

**Bound for GNNs.** Finally, with an additional technical assumption (Assumption 4) that the maximum L2 norm of aggregated node features does not grow in terms of the number of training samples, we obtain a subgroup generalization bound for GNNs in Theorem 3. The proof of Theorem 3 can be found in Appendix A.4.

**Assumption 4.** Define  $B_m := \max_{i \in V_0 \cup V_m} \|g_i(X, G)\|_2$ . For any classifier  $\tilde{h} \in \mathcal{H}$  with parameters  $\{\tilde{W}_l\}_{l=1}^L$ , assume  $\|\tilde{W}_l\|_F \leq C$  for  $l = 1, \dots, L$ . Assume  $B_m, C$  are constants with respect to  $N_0$ .

**Theorem 3** (Subgroup Generalization Bound for GNNs). Let  $\tilde{h}$  be any classifier in  $\mathcal{H}$  with parameters  $\{\tilde{W}_l\}_{l=1}^L$ . Under Assumptions 1, 2, 3, and 4, for any  $0 < m \leq M$ ,  $\gamma \geq 0$ , and large enough  $N_0$ , with probability at least  $1 - \delta$  over the sample of  $y^0$ , we have

$$\mathcal{L}_m^0(\tilde{h}) \leq \hat{\mathcal{L}}_0^\gamma(\tilde{h}) + O\left(cK\epsilon_m + \frac{b \sum_{l=1}^L \|\tilde{W}_l\|_F^2}{(\gamma/8)^{2/L} N_0^\alpha} (\epsilon_m)^{2/L} + \frac{1}{N_0^{1-2\alpha}} + \frac{1}{N_0^{2\alpha}} \ln \frac{LC(2B_m)^{1/L}}{\gamma^{1/L} \delta}\right). \quad (6)$$

Next, we investigate the qualitative implications of our theoretical results.

### 4.3 Implications for Fairness of Graph Neural Networks

**Theoretically predictable accuracy disparity.** One merit of our analysis is that we can apply Theorem 3 on different subgroups of the unlabeled nodes and compare the subgroup generalization bounds. This allows us to study the accuracy disparity across subgroups from a theoretical perspective.

A major factor that affects the generalization bound (6) is  $\epsilon_m$ , the aggregated-feature distance (in terms of  $g(X, G)$ ) from the target test subgroup  $V_m$  to the training set  $V_0$ . The generalization bound (6) suggests that there is a better generalization guarantee for subgroups that are closer to the training set. In other words, it is unfair for subgroups that are far away from the training set. While our theoretical analysis can only tell the difference among *upper bounds* of generalization errors, we empirically verify that, in the following Section 5, the aggregated-feature distance  $\epsilon_m$  is indeed a strong predictor for the test accuracy of each subgroup  $V_m$ . More specifically, the test accuracy decreases as the distance increases, which is consistent with the theoretical prediction given by the bound (6).

**Impact of the structural positions of nodes.** We further investigate if the aggregated-feature distance can be related to simpler and more interpretable graph characteristics, in order to obtain a more intuitive understanding of how the structural positions of nodes influence the prediction accuracy on them. We find that the *geodesic distance* (length of the shortest path) between two nodes is positively related to the distance between their aggregated features in some scenarios<sup>9</sup>, such as when the node features exhibit homophily [28]. Empirically, we also observe that test nodes with larger geodesic distance to the training set tend to suffer from lower accuracy (see Figure 2).

In contrast, we find that common node centrality metrics (e.g., degree and PageRank) have less influence on the test accuracy (see Figure 3). These centrality metrics only capture the graph characteristics of the test nodes alone, but do not take their relationship to the training set into account, which is a key factor suggested by our theoretical analysis.

**Impact of training data selection.** Another implication of the theoretical results is that the selection of the training set plays an important role in the fairness of the learned GNN models. First, if the training set is selected unevenly on the graph, leaving part of the test nodes far away, there will likely be a large accuracy disparity. Second, a key ingredient in the proof of Lemma 1 is that the GNN predictions on two nodes tend to be more similar if they are closer in terms of the aggregated node features. This suggests that, if an individual training node is close to many test nodes, it may bias the predictions of the learned GNN on the test nodes towards the class it belongs to.

## 5 Experiments

In this section, we empirically verify the fairness implications suggested by our theoretical analysis.

**General setup.** We experiment on 4 popular GNN models, GCN [20], GAT [41], SGC [45], and APPNP [21], as well as an MLP model for reference. For all models, we use the implementations by Deep Graph Library [43]. For each experiment setting, 40 independent trials are carried out.

### 5.1 Accuracy Disparity Across Subgroups

**Subgroups.** We examine the accuracy disparity with three types of subgroups as described below.

<sup>9</sup>A more detailed discussion on such scenarios is provided in Appendix D.1.

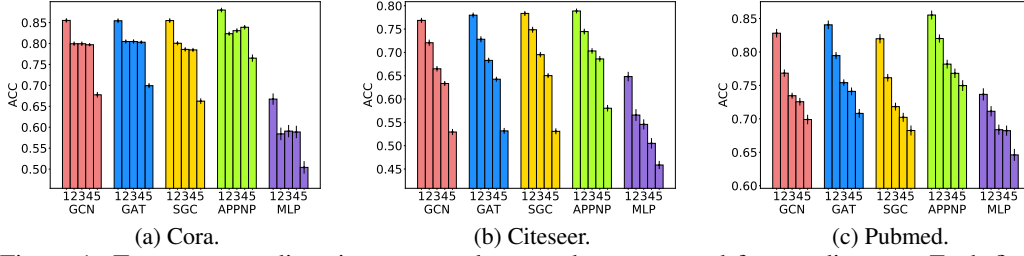


Figure 1: Test accuracy disparity across subgroups by aggregated-feature distance. Each figure corresponds to a dataset, and each bar cluster corresponds to a model. Bars labeled 1 to 5 represent subgroups with increasing distance to training set. Results are averaged over 40 independent trials with different random splits of the data, and the error bar represents the standard error of the mean.

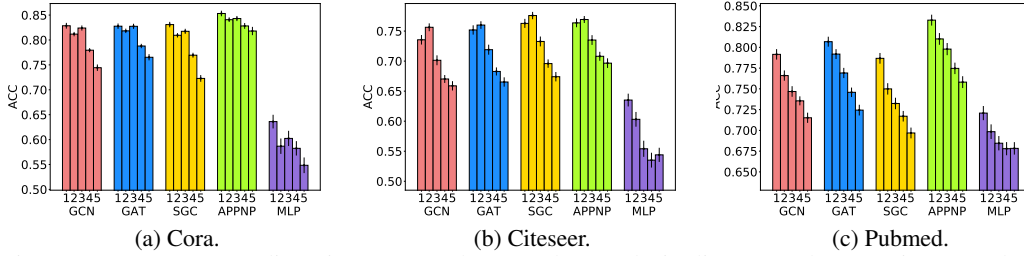


Figure 2: Test accuracy disparity across subgroups by geodesic distance. The experiment and plot settings are the same as Figure 1, except for the bars labeled from 1 to 5 here represent subgroups with increasing shortest-path distance to training set.

*Subgroup by aggregated-feature distance.* In order to directly investigate the effect of  $\epsilon_m$  on the generalization bound (6), we first split the test nodes into subgroups by their distance to the training set in terms of the aggregated features. We use the two-step aggregated features to calculate the distance. In particular, denote the adjacency matrix of the graph  $G$  as  $A \in \{0, 1\}^{N \times N}$  and the corresponding degree matrix as  $D$ , where  $D$  is an  $N \times N$  diagonal matrix with  $D_{ii} = \sum_{j=1}^N A_{ij}, \forall i = 1, \dots, N$ . Given the feature matrix  $X \in \mathbb{R}^{N \times D}$ , the two-step aggregated features  $Z$  are obtained by  $Z = (D + I)^{-1}(A + I)(D + I)^{-1}(A + I)X$ . For each test node  $i$ , we calculate its aggregated-feature distance to the training set  $V_0$  as  $d_i = \min_{j \in V_0} \|Z_i - Z_j\|_2$ . Then we sort the test nodes according to this distance and split them into 5 equal-sized subgroups.

Strictly speaking, our theory does not directly apply to GCN and GAT as they are not in the form as we defined in Section 4.2. Moreover, the two-step aggregated feature does not match exactly to the feature aggregation function of SGC and APPNP. Nevertheless, we find that even with such approximations, we are still able to observe the expected descending trend of test accuracy with respect to increasing distance in terms of the two-step aggregated features, on all four GNN models.

*Subgroup by geodesic distance.* As we discussed in Section 4.3, geodesic distance on the graph may well relate to the aggregated-feature distance. So we also define subgroups based on geodesic distance. We split the subgroups by replacing the aggregated-feature distance  $d_i$  of each test node  $i$  with the minimum of the geodesic distances from  $i$  to each training node on the graph.

*Subgroup by node centrality.* Lastly, we define subgroups based on 4 types of common node centrality metrics (degree, closeness, betweenness, and PageRank) of the test nodes. We split the subgroups by replacing the aggregated-feature distance  $d_i$  of each test node  $i$  with the centrality score of  $i$ . The purpose of this setup is to show that the common node centrality metrics are not sufficient to capture the monotonic trend of test accuracy.

**Experiment setup.** Following common GNN experiment setup [38], we randomly select 20 nodes in each class for training, 500 nodes for validation, and 1,000 nodes for testing. Once training is done,



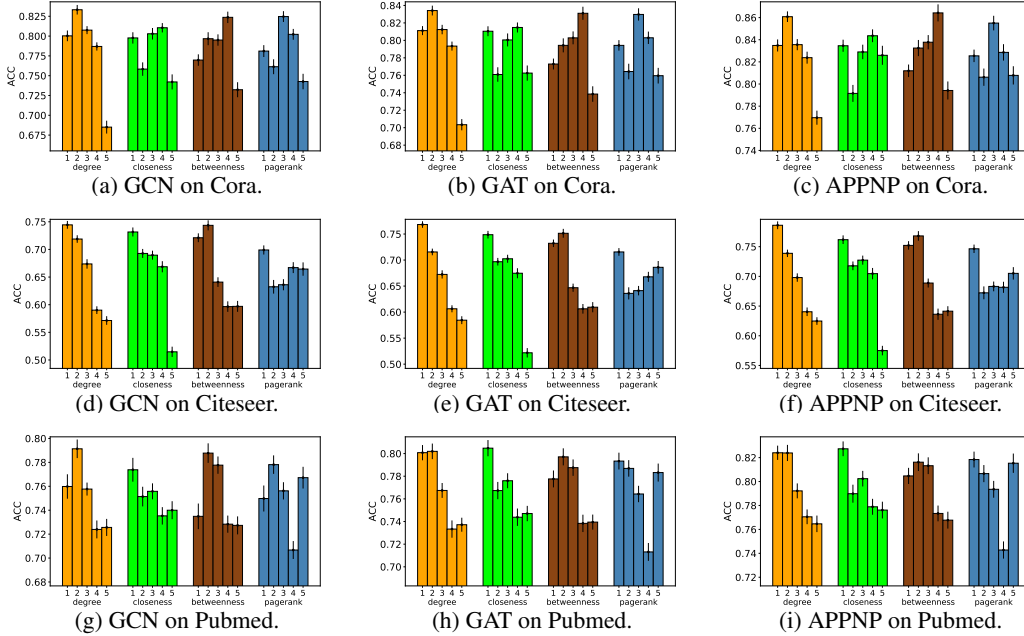


Figure 3: Test accuracy disparity across subgroups by node centrality. Each figure corresponds to the results of a pair of model and dataset, and each bar cluster corresponds to the subgroups defined by a certain centrality metric. In each cluster, the bars labeled from 1 to 5 represent subgroups with decreasing node centrality. Other settings are the same as Figure 1.

we report the test accuracy on subgroups defined by aggregated-feature distance, geodesic distance, and node centrality in Figure 1, 2, and 3 respectively<sup>10</sup>.

**Experiment results.** First, as shown in Figure 1, there is a clear trend that the accuracy of a test subgroup decreases as the aggregated-feature distance between the test subgroup and the training set increases. And the trend is consistent for all 4 GNN models on all the datasets we test on (except for APPNP on Cora). This result verifies the existence of accuracy disparity suggested by Theorem 3.

Second, we observe in Figure 2 that there is a similar trend when we split subgroups by the geodesic distance. This suggests that the geodesic distance on the graph can sometimes be used as a simpler indicator in practice for machine learning fairness on graph-structured data. Using such a classical graph metric as an indicator also helps us connect graph-based machine learning to network theory, especially to understandings about social networks, to better analyze fairness issues of machine learning on social networks, where high-stake decisions related to human subjects may be involved.

Furthermore, as shown in Figure 3, there is no clear monotonic trend for test accuracy when we split subgroups by node centrality, except for some particular combinations of GNN model and dataset. Empirically, the common node centrality metrics are not as good as the geodesic distance in terms of capturing the accuracy disparity. This contrast highlights the importance of the insight provided by our analysis: the “distance” to the training set, rather than some graph characteristics of the test nodes alone, is the key predictor of test accuracy.

Finally, it is intriguing that, in both Figure 1 and 2, the test accuracy of MLP (which does not use the graph structure) also decreases as the distance of a subgroup to the training set increases. This result is perhaps not surprising if the subgroups were defined by distance on the original node features, as MLP can be viewed as a special GNN where the feature aggregation function is an identity mapping, so the “aggregated features” for MLP essentially equal to the original features. Our theoretical analysis can then be similarly applied to MLP. The question is why there is also an accuracy disparity w.r.t. the aggregated-feature distance and the geodesic distance. We suspect this is because these datasets present homophily, i.e., original (non-aggregated) features of geodesically closer nodes tend to be more similar. As a result, a subgroup with smaller geodesic distance may also have closer node

<sup>10</sup>The main paper reports the results on a small set of datasets (Cora, Citeseer, and Pubmed [37, 47]). Results on more datasets, including large-scale datasets from Open Graph Benchmark [17], are shown in Appendix C.

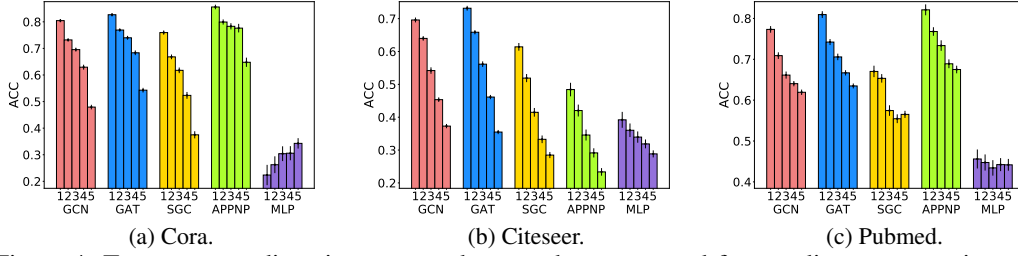


Figure 4: Test accuracy disparity across subgroups by aggregated-feature distance, experimented with noisy features. The experiment and plot settings are the same as Figure 1, except for the node features are perturbed by independent noises such that they are less homophilous.

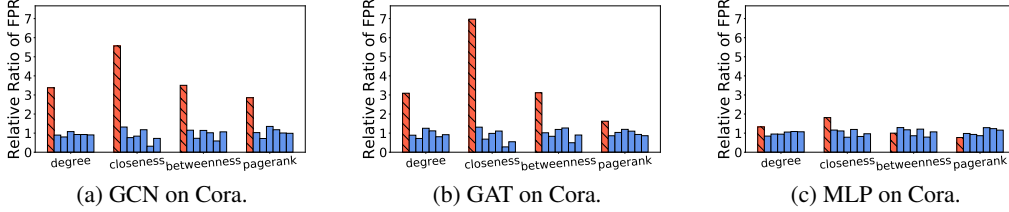


Figure 5: Relative ratio between the FPR under biased training node selection and the FPR under uniform training node selection. Each bar in each cluster corresponds to a class (there are 7 classes in total). The red shaded bar indicates the class with high centrality training nodes under the biased setup. Each cluster corresponds to a centrality metric being used for the biased node selection.

features to the training set. To verify this hypothesis, we repeat the experiments in Figure 1, but with independent noises added to node features such that they become less homophilous. As in Figure 4, the decreasing pattern of test accuracy across subgroups remains for the 4 GNNs on all datasets; while for MLP, the pattern disappears on Cora and Pubmed and becomes less sharp on Citeseer.

## 5.2 Impact of Biased Training Node Selection

In all the previous experiments, we follow the standard GNN training setup where 20 training nodes are uniformly sampled for each class. Next we investigate the impact if the selection of training nodes is biased, verifying our discussions in Section 4.3. We will demonstrate that the node centrality scores of the training nodes play an important role in the learned GNN model.

We choose a “dominant class” and construct a manipulated training set. For each class, we still sample 20 training nodes but in a biased way. For the dominant class, the sample is biased towards nodes of high centrality; while for other classes, the sample is biased towards nodes of low centrality. We evaluate the relative ratio of False Positive Rate (FPR) for each class between the setup using the manipulated training set and the setup using a uniformly sampled training set.

As shown in Figure 5, compared to MLP, the GNN models have significantly worse FPR for the dominant class when the training nodes are biased. This is because, after feature aggregation, there will be a larger proportion of test nodes that are closer to the training nodes of higher centrality. And the learned GNN model will be heavily biased towards the training labels of these nodes.

## 6 Conclusion

We present a novel PAC-Bayesian analysis for the generalization ability of GNNs on node-level semi-supervised learning tasks. As far as we know, this is the first generalization bound for GNNs for non-IID node-level tasks without strong assumptions on the data generating mechanism. One advantage of our analysis is that it can be applied to arbitrary subgroups of the test nodes, which allows us to investigate an accuracy-disparity style of fairness for GNNs. Both the theoretical and empirical results suggest that there is an accuracy disparity across subgroups of test nodes that have varying distance to the training set, and nodes with larger distance to the training nodes suffer from a lower classification accuracy. In the future, we would like to utilize our theory to analyze the fairness of GNNs on real-world applications and develop principled methods to mitigate the unfairness.

## Acknowledgements

This work was in part supported by the National Science Foundation under grant number 1633370. The authors claim no competing interests.

## References

- [1] Chirag Agarwal, Himabindu Lakkaraju, and Marinka Zitnik. Towards a unified framework for fair and stable graph representation learning. *CoRR*, abs/2102.13186, 2021. URL <https://arxiv.org/abs/2102.13186>.
- [2] Pierre Alquier, James Ridgway, and Nicolas Chopin. On the properties of variational approximations of gibbs posteriors. *The Journal of Machine Learning Research*, 17(1):8374–8414, 2016.
- [3] Aseem Baranwal, Kimon Fountoulakis, and Aukosh Jagannath. Graph convolution for semi-supervised classification: Improved linear separability and out-of-distribution generalization. *arXiv preprint arXiv:2102.06966*, 2021.
- [4] Luc Bégin, Pascal Germain, François Laviolette, and Jean-Francis Roy. Pac-bayesian theory for transductive learning. In *Artificial Intelligence and Statistics*, pages 105–113. PMLR, 2014.
- [5] Avishek Joey Bose and William L. Hamilton. Compositional fairness constraints for graph embeddings. *CoRR*, abs/1905.10674, 2019. URL <http://arxiv.org/abs/1905.10674>.
- [6] Maarten Buyl and Tijl De Bie. The kl-divergence between a graph model and its fair i-projection as a fairness regularizer. *CoRR*, abs/2103.01846, 2021. URL <https://arxiv.org/abs/2103.01846>.
- [7] Enyan Dai and Suhang Wang. Say no to the discrimination: Learning fair graph neural networks with limited sensitive attribute information. In *Proceedings of the 14th ACM International Conference on Web Search and Data Mining*, WSDM ’21, page 680–688, New York, NY, USA, 2021. Association for Computing Machinery. ISBN 9781450382977. doi: 10.1145/3437963.3441752. URL <https://doi.org/10.1145/3437963.3441752>.
- [8] Yash Deshpande, Subhabrata Sen, Andrea Montanari, and Elchanan Mossel. Contextual stochastic block models. In *NeurIPS*, 2018.
- [9] Simon S Du, Kangcheng Hou, Barnabás Póczos, Ruslan Salakhutdinov, Ruosong Wang, and Keyulu Xu. Graph neural tangent kernel: Fusing graph neural networks with graph kernels. *arXiv preprint arXiv:1905.13192*, 2019.
- [10] Gintare Karolina Dziugaite, Kyle Hsu, Waseem Gharbieh, Gabriel Arpino, and Daniel Roy. On the role of data in pac-bayes. In *International Conference on Artificial Intelligence and Statistics*, pages 604–612. PMLR, 2021.
- [11] Vikas Garg, Stefanie Jegelka, and Tommi Jaakkola. Generalization and representational limits of graph neural networks. In *International Conference on Machine Learning*, pages 3419–3430. PMLR, 2020.
- [12] Pascal Germain, Alexandre Lacasse, Francois Laviolette, Mario March, and Jean-Francis Roy. Risk bounds for the majority vote: From a pac-bayesian analysis to a learning algorithm. *Journal of Machine Learning Research*, 16(26):787–860, 2015.
- [13] Marco Gori, Gabriele Monfardini, and Franco Scarselli. A new model for learning in graph domains. In *Proceedings. 2005 IEEE International Joint Conference on Neural Networks, 2005.*, volume 2, pages 729–734. IEEE, 2005.
- [14] Benjamin Guedj. A primer on pac-bayesian learning. *arXiv preprint arXiv:1901.05353*, 2019.
- [15] Wassily Hoeffding. Probability inequalities for sums of bounded random variables. In *The Collected Works of Wassily Hoeffding*, pages 409–426. Springer, 1994.

- [16] Yifan Hou, Jian Zhang, James Cheng, Kaili Ma, Richard TB Ma, Hongzhi Chen, and Ming-Chang Yang. Measuring and improving the use of graph information in graph neural networks. In *International Conference on Learning Representations*, 2019.
- [17] Weihua Hu, Matthias Fey, Marinka Zitnik, Yuxiao Dong, Hongyu Ren, Bowen Liu, Michele Catasta, and Jure Leskovec. Open graph benchmark: Datasets for machine learning on graphs. *arXiv preprint arXiv:2005.00687*, 2020.
- [18] Wengong Jin, Regina Barzilay, and Tommi Jaakkola. Junction tree variational autoencoder for molecular graph generation. In *International Conference on Machine Learning*, pages 2323–2332. PMLR, 2018.
- [19] Ahmad Khajehnejad, Moein Khajehnejad, Mahmoudreza Babaei, Krishna P. Gummadi, Adrian Weller, and Baharan Mirzasoleiman. Crosswalk: Fairness-enhanced node representation learning, 2021.
- [20] Thomas N Kipf and Max Welling. Semi-supervised classification with graph convolutional networks. *arXiv preprint arXiv:1609.02907*, 2016.
- [21] Johannes Klicpera, Aleksandar Bojchevski, and Stephan Günnemann. Predict then propagate: Graph neural networks meet personalized pagerank. In *ICLR*, 2019.
- [22] Charlotte Laclau, Ievgen Redko, Manvi Choudhary, and Christine Largeron. All of the fairness for edge prediction with optimal transport. *CoRR*, abs/2010.16326, 2020. URL <https://arxiv.org/abs/2010.16326>.
- [23] John Langford and John Shawe-Taylor. Pac-bayes & margins. *Advances in neural information processing systems*, pages 439–446, 2003.
- [24] Qimai Li, Zhichao Han, and Xiao-Ming Wu. Deeper insights into graph convolutional networks for semi-supervised learning. In *Proceedings of the AAAI Conference on Artificial Intelligence*, volume 32, 2018.
- [25] Renjie Liao, Raquel Urtasun, and Richard Zemel. A pac-bayesian approach to generalization bounds for graph neural networks. In *ICLR*, 2021.
- [26] Yao Ma, Xiaorui Liu, Neil Shah, and Jiliang Tang. Is homophily a necessity for graph neural networks? *arXiv preprint arXiv:2106.06134*, 2021.
- [27] David McAllester. Simplified pac-bayesian margin bounds. In *Learning theory and Kernel machines*, pages 203–215. Springer, 2003.
- [28] Miller McPherson, Lynn Smith-Lovin, and James M Cook. Birds of a feather: Homophily in social networks. *Annual review of sociology*, 27(1):415–444, 2001.
- [29] Federico Monti, Davide Boscaini, Jonathan Masci, Emanuele Rodola, Jan Svoboda, and Michael M Bronstein. Geometric deep learning on graphs and manifolds using mixture model cnns. In *Proceedings of the IEEE conference on computer vision and pattern recognition*, pages 5115–5124, 2017.
- [30] Behnam Neyshabur, Srinadh Bhojanapalli, and Nathan Srebro. A pac-bayesian approach to spectrally-normalized margin bounds for neural networks. 2018.
- [31] Hoang NT and Takanori Maehara. Revisiting graph neural networks: All we have is low-pass filters. *arXiv preprint arXiv:1905.09550*, 2019.
- [32] Tahleen Rahman, Bartłomiej Surma, Michael Backes, and Yang Zhang. Fairwalk: Towards fair graph embedding. In *Proceedings of the Twenty-Eighth International Joint Conference on Artificial Intelligence, IJCAI-19*, pages 3289–3295. International Joint Conferences on Artificial Intelligence Organization, 7 2019. doi: 10.24963/ijcai.2019/456. URL <https://doi.org/10.24963/ijcai.2019/456>.
- [33] Omar Rivasplata. Subgaussian random variables: An expository note. *Internet publication, PDF*, 2012.

- [34] Ryoma Sato. A survey on the expressive power of graph neural networks. *arXiv preprint arXiv:2003.04078*, 2020.
- [35] Franco Scarselli, Marco Gori, Ah Chung Tsoi, Markus Hagenbuchner, and Gabriele Monfardini. The graph neural network model. *IEEE transactions on neural networks*, 20(1):61–80, 2008.
- [36] Franco Scarselli, Ah Chung Tsoi, and Markus Hagenbuchner. The vapnik–chervonenkis dimension of graph and recursive neural networks. *Neural Networks*, 108:248–259, 2018.
- [37] Prithviraj Sen, Galileo Namata, Mustafa Bilgic, Lise Getoor, Brian Galligher, and Tina Eliassi-Rad. Collective classification in network data. *AI magazine*, 29(3):93–93, 2008.
- [38] Oleksandr Shchur, Maximilian Mumme, Aleksandar Bojchevski, and Stephan Günnemann. Pitfalls of graph neural network evaluation. *CoRR*, abs/1811.05868, 2018. URL <http://arxiv.org/abs/1811.05868>.
- [39] Indro Spinelli, Simone Scardapane, Amir Hussain, and Aurelio Uncini. Biased edge dropout for enhancing fairness in graph representation learning, 2021.
- [40] Joel A Tropp. An introduction to matrix concentration inequalities. *Foundations and Trends in Machine Learning*, 8(1-2):1–230, 2015.
- [41] Petar Veličković, Guillem Cucurull, Arantxa Casanova, Adriana Romero, Pietro Liò, and Yoshua Bengio. Graph attention networks. In *ICLR*, 2018.
- [42] Saurabh Verma and Zhi-Li Zhang. Stability and generalization of graph convolutional neural networks. In *Proceedings of the 25th ACM SIGKDD International Conference on Knowledge Discovery & Data Mining*, pages 1539–1548, 2019.
- [43] Minjie Wang, Da Zheng, Zihao Ye, Quan Gan, Mufei Li, Xiang Song, Jinjing Zhou, Chao Ma, Lingfan Yu, Yu Gai, et al. Deep graph library: A graph-centric, highly-performant package for graph neural networks. *arXiv preprint arXiv:1909.01315*, 2019.
- [44] Duncan J Watts and Steven H Strogatz. Collective dynamics of ‘small-world’ networks. *nature*, 393(6684):440–442, 1998.
- [45] Felix Wu, Amauri Souza, Tianyi Zhang, Christopher Fifty, Tao Yu, and Kilian Weinberger. Simplifying graph convolutional networks. In *International conference on machine learning*, pages 6861–6871. PMLR, 2019.
- [46] Zonghan Wu, Shirui Pan, Fengwen Chen, Guodong Long, Chengqi Zhang, and S Yu Philip. A comprehensive survey on graph neural networks. *IEEE transactions on neural networks and learning systems*, 2020.
- [47] Zhilin Yang, William Cohen, and Ruslan Salakhudinov. Revisiting semi-supervised learning with graph embeddings. In *International conference on machine learning*, pages 40–48. PMLR, 2016.
- [48] Rex Ying, Ruining He, Kaifeng Chen, Pong Eksombatchai, William L Hamilton, and Jure Leskovec. Graph convolutional neural networks for web-scale recommender systems. In *Proceedings of the 24th ACM SIGKDD International Conference on Knowledge Discovery & Data Mining*, pages 974–983, 2018.
- [49] Bing Yu, Haoteng Yin, and Zhanxing Zhu. Spatio-temporal graph convolutional networks: a deep learning framework for traffic forecasting. In *Proceedings of the 27th International Joint Conference on Artificial Intelligence*, pages 3634–3640, 2018.
- [50] Ziqian Zeng, Rashidul Islam, Kamrun Naher Keya, James R. Foulds, Yangqiu Song, and Shimei Pan. Fair representation learning for heterogeneous information networks. *CoRR*, abs/2104.08769, 2021. URL <https://arxiv.org/abs/2104.08769>.
- [51] Wenda Zhou, Victor Veitch, Morgane Austern, Ryan P Adams, and Peter Orbanz. Non-vacuous generalization bounds at the imagenet scale: a pac-bayesian compression approach. In *International Conference on Learning Representations*, 2018.

- [52] Jiong Zhu, Yujun Yan, Lingxiao Zhao, Mark Heimann, Leman Akoglu, and Danai Koutra. Beyond homophily in graph neural networks: Current limitations and effective designs. *Advances in Neural Information Processing Systems*, 33, 2020.

## Contents

<b>1</b>	<b>Introduction</b>	<b>1</b>
<b>2</b>	<b>Related Work</b>	<b>2</b>
2.1	Generalization of Graph Neural Networks . . . . .	2
2.2	Fairness of Machine Learning on Graphs . . . . .	2
2.3	PAC-Bayesian Analysis . . . . .	2
<b>3</b>	<b>Preliminaries</b>	<b>3</b>
3.1	The Problem Formulation and Notations . . . . .	3
3.2	The PAC-Bayesian Framework . . . . .	4
<b>4</b>	<b>The Generalization Bound and Its Implications for Fairness</b>	<b>4</b>
4.1	General PAC-Bayesian Theorems for Subgroup Generalization . . . . .	4
4.2	Subgroup Generalization Bound for Graph Neural Networks . . . . .	5
4.3	Implications for Fairness of Graph Neural Networks . . . . .	7
<b>5</b>	<b>Experiments</b>	<b>7</b>
5.1	Accuracy Disparity Across Subgroups . . . . .	7
5.2	Impact of Biased Training Node Selection . . . . .	10
<b>6</b>	<b>Conclusion</b>	<b>10</b>
<b>A</b>	<b>Proofs</b>	<b>17</b>
A.1	Proof of Theorem 1 . . . . .	17
A.2	Proof of Theorem 2 . . . . .	18
A.3	Proof of Lemma 1 . . . . .	19
A.4	Proof of Theorem 3 . . . . .	21
A.5	Discussion on Assumption 3 . . . . .	23
<b>B</b>	<b>More Details of Experiment Setup</b>	<b>25</b>
B.1	Detailed Training Setup . . . . .	25
B.2	Detailed Setup of the Noisy Feature Experiment . . . . .	25
B.3	Detailed Setup of the Biased Training Node Selection Experiment . . . . .	26
<b>C</b>	<b>Extra Experiment Results</b>	<b>27</b>
C.1	Accuracy Disparity on Amazon Datasets . . . . .	27
C.2	Accuracy Disparity on Open Graph Benchmarks . . . . .	27
C.3	More Results of Biased Training Node Selection . . . . .	30
<b>D</b>	<b>Discussions</b>	<b>30</b>
D.1	Relationship Between Aggregated-Feature Distance and Geodesic Distance . . . . .	30

D.2	Implications for GNN Generalization under Non-Homophily . . . . .	31
D.3	Limitations of the Analysis . . . . .	32
D.4	Societal Impacts . . . . .	32



## A Proofs

### A.1 Proof of Theorem 1

We first introduce three lemmas whose proofs can be found in the referred literature.

**Lemma 2** (Hoeffding’s Inequality for Bounded Random Variables [15]). *Suppose  $X_1, X_2, \dots, X_n$  are independent random variables with  $a_i \leq X_i \leq b_i, \forall i = 1, 2, \dots, n$ . Let  $\bar{X} = \frac{1}{n} \sum_{i=1}^n X_i$ . Then, for any  $t > 0$ ,*

$$\Pr(|\bar{X} - \mathbb{E}\bar{X}| > t) \leq 2e^{-\frac{n^2 t^2}{\sum_{i=1}^n (b_i - a_i)^2}}.$$

**Lemma 3** (Sub-Gaussianity). *If  $X$  is a centered random variable, i.e.,  $\mathbb{E}X = 0$ , and if  $\exists \nu > 0$ , for any  $t > 0$ ,*

$$\Pr(|X| > t) \leq 2e^{-\nu t^2}.$$

Then, for any  $\lambda > 0$ ,

$$\mathbb{E}e^{\lambda X} \leq e^{\frac{\lambda^2}{2\nu}}.$$

See Rivasplata [33] (Theorem 3.1) for the proof of Lemma 3.

**Lemma 4** (Change-of-Measure Inequality, Lemma 17 in Germain et al. [12]). *For any two distributions  $P$  and  $Q$  defined on  $\mathcal{H}$ , and any function  $\psi : \mathcal{H} \rightarrow \mathbb{R}$ ,*

$$\mathbb{E}_{h \sim Q}[\psi(h)] \leq D_{\text{KL}}(Q \| P) + \ln \mathbb{E}_{h \sim P}[e^{\psi(h)}].$$

Then we can prove Theorem 1. For convenience, we re-state it as Theorem 4 below.

**Theorem 4** (Subgroup Generalization of Stochastic Classifiers). *For any  $0 < m \leq M$ , for any  $\lambda > 0$  and  $\gamma \geq 0$ , for any “prior” distribution  $P$  on  $\mathcal{H}$  that is independent of the training data on  $V_0$ , with probability at least  $1 - \delta$  over the sample of  $y^0$ , for any  $Q$  on  $\mathcal{H}$ , we have<sup>11</sup>*

$$\mathcal{L}_m^{\gamma/2}(Q) \leq \hat{\mathcal{L}}_0^\gamma(Q) + \frac{1}{\lambda} \left( D_{\text{KL}}(Q \| P) + \ln \frac{1}{\delta} + \frac{\lambda^2}{4N_0} + D_{m,0}^\gamma(P; \lambda) \right). \quad (7)$$

*Proof.* We prove the result by upper-bounding the quantity  $\lambda(\mathcal{L}_m^{\gamma/2}(Q) - \hat{\mathcal{L}}_0^\gamma(Q))$ . First, we have

$$\begin{aligned} & \lambda(\mathcal{L}_m^{\gamma/2}(Q) - \hat{\mathcal{L}}_0^\gamma(Q)) \\ & \leq \mathbb{E}_{h \sim Q} \lambda(\mathcal{L}_m^{\gamma/2}(h) - \hat{\mathcal{L}}_0^\gamma(h)) \\ & \leq D_{\text{KL}}(Q \| P) + \ln \mathbb{E}_{h \sim P} e^{\lambda(\mathcal{L}_m^{\gamma/2}(h) - \hat{\mathcal{L}}_0^\gamma(h))}, \end{aligned} \quad (8)$$

where the first inequality is due to Jensen’s inequality, and the last inequality is due to Lemma 4.

Next we would like to upper-bound the second term in the RHS of (8). Note that the quantity  $U := \mathbb{E}_{h \sim P} e^{\lambda(\mathcal{L}_m^{\gamma/2}(h) - \hat{\mathcal{L}}_0^\gamma(h))}$  is a random variable with the randomness coming from the sample of node labels  $y^0$  for  $V_0$ . Also note that  $P$  is independent of  $y^0$ . Applying Markov’s inequality to  $U$ , we have for any  $\delta > 0$ , with probability at least  $1 - \delta$  over the sample of  $y^0$ ,

$$U \leq \frac{1}{\delta} \mathbb{E}_{y^0} U,$$

and hence,

$$\ln U \leq \ln \frac{1}{\delta} \mathbb{E}_{y^0} U = \ln \frac{1}{\delta} + \ln \mathbb{E}_{y^0} U.$$

Then we need to upper-bound the quantity  $\ln \mathbb{E}_{y^0} U$ . We can re-write it as

$$\ln \mathbb{E}_{y^0} U = \ln \mathbb{E}_{y^0} \mathbb{E}_{h \sim P} e^{\lambda(\mathcal{L}_m^{\gamma/2}(h) - \hat{\mathcal{L}}_0^\gamma(h))} = \ln \mathbb{E}_{h \sim P} \mathbb{E}_{y^0} e^{\lambda(\mathcal{L}_m^{\gamma/2}(h) - \hat{\mathcal{L}}_0^\gamma(h))}. \quad (9)$$

<sup>11</sup>Theorem 4 also holds when we substitute  $\mathcal{L}_m^{\gamma/2}(h)$  and  $\mathcal{L}_m^{\gamma/2}(Q)$  as  $\mathcal{L}_m^\gamma(h)$  and  $\mathcal{L}_m^\gamma(Q)$  respectively. But we state the theorem in this form to ease the development of the later analysis.

For a fixed model  $h$ ,

$$\begin{aligned}
& \mathbb{E}_{y^0} e^{\lambda(\mathcal{L}_m^{\gamma/2}(h) - \widehat{\mathcal{L}}_0^\gamma(h))} \\
&= \mathbb{E}_{y^0} e^{\lambda(\mathcal{L}_m^{\gamma/2}(h) - \mathcal{L}_0^\gamma(h) + \mathcal{L}_0^\gamma(h) - \widehat{\mathcal{L}}_0^\gamma(h))} \\
&= \mathbb{E}_{y^0} e^{\lambda(\mathcal{L}_m^{\gamma/2}(h) - \mathcal{L}_0^\gamma(h))} e^{\lambda(\mathcal{L}_0^\gamma(h) - \widehat{\mathcal{L}}_0^\gamma(h))} \\
&= e^{\lambda(\mathcal{L}_m^{\gamma/2}(h) - \mathcal{L}_0^\gamma(h))} \mathbb{E}_{y^0} e^{\lambda(\mathcal{L}_0^\gamma(h) - \widehat{\mathcal{L}}_0^\gamma(h))}. \tag{10}
\end{aligned}$$

In the following we will give an upper bound on  $\mathbb{E}_{y^0} e^{\lambda(\mathcal{L}_0^\gamma(h) - \widehat{\mathcal{L}}_0^\gamma(h))}$  that is independent of  $h$ . Recall that

$$\widehat{\mathcal{L}}_0^\gamma(h) = \frac{1}{N_0} \sum_{i \in V_0} \mathbb{1} \left[ h_i(X, G)[y_i] \leq \gamma + \max_{k \neq y_i} h_i(X, G)[k] \right],$$

where the node labels are independently sampled (though not from the identical distribution), so  $\widehat{\mathcal{L}}_0^\gamma(h)$  is the empirical mean of  $N_0$  independent Bernoulli random variables and  $\mathcal{L}_0^\gamma(h)$  is the expectation of  $\widehat{\mathcal{L}}_0^\gamma(h)$ . By Lemma 2, for any  $t > 0$ ,

$$\Pr(|\mathcal{L}_0^\gamma(h) - \widehat{\mathcal{L}}_0^\gamma(h)| \geq t) \leq 2e^{-2N_0 t^2},$$

and hence  $\mathcal{L}_0^\gamma(h) - \widehat{\mathcal{L}}_0^\gamma(h)$  is sub-Gaussian. Further by Lemma 3, we have

$$\mathbb{E}_{y^0} e^{\lambda(\mathcal{L}_0^\gamma(h) - \widehat{\mathcal{L}}_0^\gamma(h))} \leq e^{\frac{\lambda^2}{4N_0}},$$

which implies that

$$\mathbb{E}_{y^0} e^{\lambda(\mathcal{L}_0^\gamma(h) - \widehat{\mathcal{L}}_0^\gamma(h))} \leq e^{\frac{\lambda^2}{4N_0}}, \tag{11}$$

Therefore, plugging (10) and (11) back into (9), we have

$$\begin{aligned}
& \ln \mathbb{E}_{y^0} U \\
& \leq \ln \mathbb{E}_{h \sim P} e^{\lambda(\mathcal{L}_m^{\gamma/2}(h) - \mathcal{L}_0^\gamma(h))} e^{\frac{\lambda^2}{4N_0}} \\
& = D_{m,0}^\gamma(P; \lambda) + \frac{\lambda^2}{4N_0}.
\end{aligned}$$

Finally, plugging everything back into (8), we get

$$\begin{aligned}
& \lambda(\mathcal{L}_m^{\gamma/2}(Q) - \widehat{\mathcal{L}}_0^\gamma(Q)) \\
& \leq D_{\text{KL}}(Q \| P) + \ln \mathbb{E}_{h \sim P} e^{\lambda(\mathcal{L}_m^{\gamma/2}(h) - \mathcal{L}_0^\gamma(h))} \\
& \leq D_{\text{KL}}(Q \| P) + \ln \frac{1}{\delta} + \frac{\lambda^2}{4N_0} + D_{m,0}^\gamma(P; \lambda).
\end{aligned}$$

Rearranging the terms gives us the final result

$$\mathcal{L}_m^{\gamma/2}(Q) \leq \widehat{\mathcal{L}}_0^\gamma(Q) + \frac{1}{\lambda} \left( D_{\text{KL}}(Q \| P) + \ln \frac{1}{\delta} + \frac{\lambda^2}{4N_0} + D_{m,0}^\gamma(P; \lambda) \right).$$

□

## A.2 Proof of Theorem 2

We re-state Theorem 2 as Theorem 5 below.

**Theorem 5** (Subgroup Generalization of Deterministic Classifiers). *Let  $\tilde{h}$  be any classifier in  $\mathcal{H}$ . For any  $0 < m \leq M$ , for any  $\lambda > 0$  and  $\gamma \geq 0$ , for any “prior” distribution  $P$  on  $\mathcal{H}$  that is independent of the training data on  $V_0$ , with probability at least  $1 - \delta$  over the sample of  $y^0$ , for any  $Q$  on  $\mathcal{H}$  such that  $\Pr_{h \sim Q} \left( \max_{i \in V_0 \cup V_m} \|h_i(X, G) - \tilde{h}_i(X, G)\|_\infty < \frac{\gamma}{8} \right) > \frac{1}{2}$ , we have*

$$\mathcal{L}_m^0(\tilde{h}) \leq \widehat{\mathcal{L}}_0^\gamma(\tilde{h}) + \frac{1}{\lambda} \left( 2(D_{\text{KL}}(Q \| P) + 1) + \ln \frac{1}{\delta} + \frac{\lambda^2}{4N_0} + D_{m,0}^{\gamma/2}(P; \lambda) \right). \tag{12}$$

*Proof.* For simplicity, we write  $h_i(X, G)$  and  $\tilde{h}_i(X, G)$  as  $h_i$  and  $\tilde{h}_i$  in this proof. We first construct a distribution  $Q'$  by restricting  $Q$  on  $\mathcal{H}_{\tilde{h}} \subseteq \mathcal{H}$ , where

$$\mathcal{H}_{\tilde{h}} := \{h \in \mathcal{H} \mid \max_{i \in V_0 \cup V_m} \|h_i - \tilde{h}_i\|_\infty < \frac{\gamma}{8}\}.$$

And  $Q'$  is defined as

$$Q'(h) = \begin{cases} \frac{1}{Z_{Q'}} Q(h), & \text{if } h \in \mathcal{H}_{\tilde{h}} \\ 0, & \text{otherwise} \end{cases},$$

where  $Z_{Q'} = \Pr_{h \sim Q}(h \in \mathcal{H}_{\tilde{h}}) \geq \frac{1}{2}$  by the condition of the theorem.

For any  $h \in \mathcal{H}_{\tilde{h}}$  and any sample  $i \in V_0 \cup V_m$ , by definition of  $\mathcal{H}_{\tilde{h}}$ , we have

$$\max_{k, k' \in \{1, \dots, K\}} |(\tilde{h}_i[k] - \tilde{h}_i[k']) - (h_i[k] - h_i[k'])| < \frac{\gamma}{4},$$

which implies the following relationships:

$$\mathcal{L}_m^0(\tilde{h}) \leq \mathcal{L}_m^{\gamma/4}(h), \quad \widehat{\mathcal{L}}_0^{\gamma/2}(h) \leq \widehat{\mathcal{L}}_0^\gamma(\tilde{h}).$$

Therefore, with probability at least  $1 - \delta$  over the sample of  $y^m$ ,

$$\begin{aligned} & \mathcal{L}_m^0(\tilde{h}) \\ & \leq \mathbb{E}_{h \sim Q'} \mathcal{L}_m^{\gamma/4}(h) \\ & \leq \mathbb{E}_{h \sim Q'} \widehat{\mathcal{L}}_0^{\gamma/2}(h) + \frac{1}{\lambda} \left( D_{\text{KL}}(Q' \| P) + \ln \frac{1}{\delta} + \frac{\lambda^2}{4N_0} + D_{m,0}^{\gamma/2}(P; \lambda) \right) \\ & \leq \widehat{\mathcal{L}}_0^\gamma(\tilde{h}) + \frac{1}{\lambda} \left( D_{\text{KL}}(Q' \| P) + \ln \frac{1}{\delta} + \frac{\lambda^2}{4N_0} + D_{m,0}^{\gamma/2}(P; \lambda) \right), \end{aligned}$$

where the second inequality is due to the application of Theorem 1 by substituting  $\gamma$  as  $\gamma/2$  and  $Q$  as  $Q'$ .

Finally, to complete the proof, we only need to show

$$D_{\text{KL}}(Q' \| P) \leq 2(D_{\text{KL}}(Q \| P) + 1).$$

Denote  $\mathcal{H}_{\tilde{h}}^c$  as the complement of  $\mathcal{H}_{\tilde{h}}$  and define  $Q'^c$  as the distribution restricted to  $\mathcal{H}_{\tilde{h}}^c$  similarly as  $Q'$ . Define  $H(x) := -x \ln x - (1-x) \ln(1-x)$ , which is the binary entropy function and we know  $H(Z) \leq 1$ . Then

$$\begin{aligned} D_{\text{KL}}(Q \| P) &= \int_{\mathcal{H}_{\tilde{h}}} \ln \frac{dQ}{dP} dQ + \int_{\mathcal{H}_{\tilde{h}}^c} \ln \frac{dQ}{dP} dQ \\ &= Z_{Q'} \int_{\mathcal{H}} \ln \frac{dQ'}{dP} dQ' + (1 - Z_{Q'}) \int_{\mathcal{H}} \ln \frac{dQ'^c}{dP} dQ'^c - H(Z_{Q'}) \\ &= Z_{Q'} D_{\text{KL}}(Q' \| P) + (1 - Z_{Q'}) D_{\text{KL}}(Q'^c \| P) - H(Z_{Q'}). \end{aligned}$$

So

$$D_{\text{KL}}(Q' \| P) = \frac{1}{Z_{Q'}} (D_{\text{KL}}(Q \| P) + H(Z_{Q'}) - (1 - Z_{Q'}) D_{\text{KL}}(Q'^c \| P)) \leq 2(D_{\text{KL}}(Q \| P) + 1),$$

since  $D_{\text{KL}}(Q'^c \| P) \geq 0$ .  $\square$

### A.3 Proof of Lemma 1

We first present the following Lemma 5 that bounds the difference between the margin loss on  $V_m$  and that on  $V_0$  for a fixed GNN.

**Lemma 5.** Suppose an  $L$ -layer GNN classifier  $h$  is associated with model parameters  $W_1, \dots, W_L$ . Define  $T_h := \max_{l=1, \dots, L} \|W_l\|_2$ . Under Assumption 1 and 2, for any  $0 < m \leq M$  and  $\gamma \geq 0$ , if  $\epsilon_m T_h^L \leq \frac{\gamma}{4}$ , then

$$\mathcal{L}_m^{\gamma/2}(h) - \mathcal{L}_0^\gamma(h) \leq cK\epsilon_m.$$

*Proof.* For simplicity in this proof, for any  $i \in V_0 \cup V_m$  and  $k = 1, \dots, K$ , we use  $h_i$  to denote  $h_i(X, G)$  and use  $\eta_k(i)$  to denote  $\Pr(y_i = k \mid g_i(X, G))$ . And define  $\mathcal{L}^\gamma(h_i, y_i) := \mathbb{1}[h_i[y_i] \leq \gamma + \max_{k \neq y_i} h_i[k]]$ . Then we can write

$$\begin{aligned} & \mathcal{L}_m^{\gamma/2}(h) - \mathcal{L}_0^\gamma(h) \\ &= \mathbb{E}_{y^m} \left[ \frac{1}{N_m} \sum_{j \in V_m} \mathcal{L}^{\gamma/2}(h_j, y_j) \right] - \mathbb{E}_{y^0} \left[ \frac{1}{N_0} \sum_{i \in V_0} \mathcal{L}^\gamma(h_i, y_i) \right] \\ &= \frac{1}{N_0} \mathbb{E}_{y^0, y^m} \sum_{i \in V_0} \frac{1}{s_m} \left( \sum_{j \in V_m^{(i)}} \mathcal{L}^{\gamma/2}(h_j, y_j) \right) - \mathcal{L}^\gamma(h_i, y_i) \end{aligned}$$

where in the last step we have used Assumption 2. Therefore,

$$\begin{aligned} & \mathcal{L}_m^{\gamma/2}(h) - \mathcal{L}_0^\gamma(h) \\ &= \frac{1}{N_0} \sum_{i \in V_0} \frac{1}{s_m} \left( \sum_{j \in V_m^{(i)}} \mathbb{E}_{y_j} \mathcal{L}^{\gamma/2}(h_j, y_j) \right) - \mathbb{E}_{y_i} \mathcal{L}^\gamma(h_i, y_i) \\ &= \frac{1}{N_0} \sum_{i \in V_0} \frac{1}{s_m} \left( \sum_{j \in V_m^{(i)}} \sum_{k=1}^K \eta_k(j) \mathcal{L}^{\gamma/2}(h_j, k) \right) - \sum_{k=1}^K \Pr(y_i = k) \mathcal{L}^\gamma(h_i, k) \\ &= \frac{1}{N_0} \sum_{i \in V_0} \frac{1}{s_m} \sum_{j \in V_m^{(i)}} \sum_{k=1}^K \left( \eta_k(j) \mathcal{L}^{\gamma/2}(h_j, k) - \eta_k(i) \mathcal{L}^\gamma(h_i, k) \right) \\ &= \frac{1}{N_0} \sum_{i \in V_0} \frac{1}{s_m} \sum_{j \in V_m^{(i)}} \sum_{k=1}^K \left( \eta_k(j) \left( \mathcal{L}^{\gamma/2}(h_j, k) - \mathcal{L}^\gamma(h_i, k) \right) + (\eta_k(j) - \eta_k(i)) \mathcal{L}^\gamma(h_i, k) \right) \quad (13) \end{aligned}$$

$$\leq \frac{1}{N_0} \sum_{i \in V_0} \frac{1}{s_m} \sum_{j \in V_m^{(i)}} \sum_{k=1}^K \left( 1 \cdot \left( \mathcal{L}^{\gamma/2}(h_j, k) - \mathcal{L}^\gamma(h_i, k) \right) + (\eta_k(j) - \eta_k(i)) \cdot 1 \right), \quad (14)$$

where the last inequality utilizes the facts that both  $\eta_k(j)$  and  $\mathcal{L}^\gamma(h_i, k)$  are upper-bounded by 1. According to Assumption 1 and 2,

$$\eta_k(j) - \eta_k(i) \leq c \|g_j(X, G) - g_i(X, G)\|_2 \leq c \epsilon_m.$$

Further, as  $h_i = f(g_i(X, G); W_1, \dots, W_L)$  where  $f$  is a ReLU-activated MLP, so

$$\|h_i - h_j\|_\infty \leq \|g_i(X, G) - g_j(X, G)\|_2 \prod_{l=1}^L \|W_l\|_2 \leq \epsilon_m T_h^L \leq \frac{\gamma}{4}.$$

This implies that, for any  $k = 1, \dots, K$ ,

$$\mathcal{L}^{\gamma/2}(h_j, k) \leq \mathcal{L}^\gamma(h_i, k).$$

So we have

$$\begin{aligned} & \mathcal{L}_m^{\gamma/2}(h) - \mathcal{L}_0^\gamma(h) \\ & \leq \frac{1}{N_0} \sum_{i \in V_0} \frac{1}{s_m} \sum_{j \in V_m^{(i)}} \sum_{k=1}^K 0 + c \epsilon_m \\ & = c K \epsilon_m. \end{aligned}$$

□

Then we can prove Lemma 1, which we re-state as Lemma 6 below.

**Lemma 6** (Bound for  $D_{m,0}^{\gamma/2}(P; \lambda)$ ). *Under Assumption 1, 2 and 3, for any  $0 < m \leq M$ , any  $0 < \lambda \leq N_0^{2\alpha}$  and  $\gamma \geq 0$ , assume the “prior”  $P$  on  $\mathcal{H}$  is defined by sampling the vectorized MLP parameters from  $\mathcal{N}(0, \sigma^2 I)$  for some  $\sigma^2 \leq \frac{(\gamma/8\epsilon_m)^{2/L}}{2b(\lambda N_0^{-\alpha} + \ln 2bL)}$ . We have*

$$D_{m,0}^{\gamma/2}(P; \lambda) \leq \ln 3 + \lambda c K \epsilon_m. \quad (15)$$

*Proof.* Recall that  $D_{m,0}^{\gamma/2}(P; \lambda) = \ln \mathbb{E}_{h \sim P} e^{\lambda(\mathcal{L}_m^{\gamma/4}(h) - \mathcal{L}_0^{\gamma/2}(h))}$ . We prove the upper bound of  $D_{m,0}^{\gamma/2}(P; \lambda)$  by decomposing the space  $\mathcal{H}$  into the two regimes: a regime with bounded spectral norms of the model parameters required by Lemma 5, and its complement. Following Lemma 5, for any classifier  $h$  with parameters  $W_1, \dots, W_L$ , we define  $T_h := \max_{l=1, \dots, L} \|W_l\|_2$ .

We first prove an upper bound on the probability  $\Pr(T_h^L \epsilon_m > \frac{\gamma}{8})$  over the drawing of  $h \sim P$ . For any  $h$ , as its vectorized MLP parameters  $\text{vec}(W_l)$ , for each  $l = 1, \dots, L$ , is sampled from  $\mathcal{N}(0, \sigma^2 I)$ , we have the following spectral norm bound [40], for any  $t > 0$ ,

$$\Pr(\|W_l\|_2 > t) \leq 2be^{-\frac{t^2}{2b\sigma^2}},$$

where  $b$  is the maximum width of all hidden layers of the MLP. Setting  $t = \left(\frac{\gamma}{8\epsilon_m}\right)^{1/L}$  and applying a union bound, we have that

$$\Pr\left(T_h^L \epsilon_m > \frac{\gamma}{8}\right) = \Pr\left(T_h > \left(\frac{\gamma}{8\epsilon_m}\right)^{1/L}\right) \leq 2bLe^{-\frac{(\gamma/8\epsilon_m)^{2/L}}{2b\sigma^2}} \leq e^{-\lambda N_0^{-\alpha}},$$

where the last inequality utilizes the condition  $\sigma^2 \leq \frac{(\gamma/8\epsilon_m)^{2/L}}{2b(\lambda N_0^{-\alpha} + \ln 2bL)}$ .

For any  $h$  satisfying  $T_h^L \epsilon_m \leq \frac{\gamma}{8}$ , by Lemma 5, we know that  $e^{\lambda(\mathcal{L}_m^{\gamma/4}(h) - \mathcal{L}_0^{\gamma/2}(h))} \leq e^{\lambda c K \epsilon_m}$ . For all  $h$  such that  $T_h^L \epsilon_m > \frac{\gamma}{8}$ , by Assumption 3, with probability at least  $1 - e^{-N_0^{2\alpha}}$ ,

$$e^{\lambda(\mathcal{L}_m^{\gamma/4}(h) - \mathcal{L}_0^{\gamma/2}(h))} \leq e^{\lambda N_0^{-\alpha} + \lambda c K \epsilon_m}.$$

Also note that  $\mathcal{L}_m^{\gamma/4}(h) - \mathcal{L}_0^{\gamma/2}(h) \leq 1$  trivially holds for any  $h$ . Therefore we have

$$\begin{aligned} & D_{m,0}^{\gamma/2}(P; \lambda) \\ &= \ln \mathbb{E}_{h \sim P} e^{\lambda(\mathcal{L}_m^{\gamma/4}(h) - \mathcal{L}_0^{\gamma/2}(h))} \\ &\leq \ln \left( \Pr\left(T_h^L \epsilon_m > \frac{\gamma}{8}\right) \left( e^{-N_0^{2\alpha}} \cdot e^{\lambda} + (1 - e^{-N_0^{2\alpha}}) \cdot e^{\lambda N_0^{-\alpha} + \lambda c K \epsilon_m} \right) + \Pr\left(T_h^L \epsilon_m \leq \frac{\gamma}{8}\right) e^{\lambda c K \epsilon_m} \right) \\ &\leq \ln \left( e^{\lambda - N_0^{2\alpha}} + \Pr\left(T_h^L \epsilon_m > \frac{\gamma}{8}\right) e^{\lambda N_0^{-\alpha}} e^{\lambda c K \epsilon_m} + e^{\lambda c K \epsilon_m} \right) \\ &\leq \ln \left( 1 + e^{-\lambda N_0^{-\alpha}} e^{\lambda N_0^{-\alpha}} e^{\lambda c K \epsilon_m} + e^{\lambda c K \epsilon_m} \right) \\ &= \ln (1 + 2e^{\lambda c K \epsilon_m}) \\ &\leq \ln 3 + \lambda c K \epsilon_m, \\ &\text{since } 1 + 2e^{\lambda c K \epsilon_m} \leq 3e^{\lambda c K \epsilon_m}. \end{aligned}$$

□

#### A.4 Proof of Theorem 3

The proof of Theorem 3 relies on the combination of Theorem 2, Lemma 1, and an intermediate result of the Theorem 1 in Neyshabur et al. [30] (which we state as Lemma 7 below).

**Lemma 7** (Neyshabur et al. [30]). *Let  $\tilde{h}$  be any classifier in  $\mathcal{H}$  with parameters  $\{\tilde{W}_l\}_{l=1}^L$ . Define  $\tilde{\beta} = \left(\prod_{l=1}^L \|\tilde{W}_l\|_2\right)^{1/L}$ . Let  $\{U_l\}_{l=1}^L$  be the random perturbation to be added to  $\{\tilde{W}_l\}_{l=1}^L$  and  $\text{vec}(\{U_l\}_{l=1}^L) \sim \mathcal{N}(0, \sigma^2 I)$ . Define  $B_m := \max_{i \in V_0 \cup V_m} \|g_i(X, G)\|_2$ . If*

$$\sigma \leq \frac{\gamma}{84LB_m\beta^{L-1}\sqrt{b\ln(4bL)}},$$

and  $\beta$  is any constant satisfying  $|\tilde{\beta} - \beta| \leq \frac{\tilde{\beta}}{L}$ , then with respect to the random draw of  $\{U_l\}_{l=1}^L$ ,

$$\Pr\left(\max_{i \in V_0 \cup V_m} \|f(g_i(X, G); \{\tilde{W}_l\}_{l=1}^L) - f(g_i(X, G); \{\tilde{W}_l + U_l\}_{l=1}^L)\|_\infty < \frac{\gamma}{8}\right) > \frac{1}{2}.$$

Then we prove Theorem 3 (re-stated as Theorem 6 below).

**Theorem 6** (Subgroup Generalization Bound for GNNs). *Let  $\tilde{h}$  be any classifier in  $\mathcal{H}$  with parameters  $\{\tilde{W}_l\}_{l=1}^L$ . Under Assumptions 1, 2, 3, and 4, for any  $0 < m \leq M$ ,  $\gamma \geq 0$ , and large enough  $N_0$ , with probability at least  $1 - \delta$  over the sample of  $y^0$ , we have*

$$\mathcal{L}_m^0(\tilde{h}) \leq \hat{\mathcal{L}}_0^\gamma(\tilde{h}) + O\left(cK\epsilon_m + \frac{b \sum_{l=1}^L \|\tilde{W}_l\|_F^2}{(\gamma/8)^{2/L} N_0^\alpha} (\epsilon_m)^{2/L} + \frac{1}{N_0^{1-2\alpha}} + \frac{1}{N_0^{2\alpha}} \ln \frac{LC(2B_m)^{1/L}}{\gamma^{1/L} \delta}\right). \quad (16)$$

*Proof.* There are two main steps in the proof. In the first step, for a given constant  $\beta > 0$ , we first define the “prior”  $P$  and the “posterior”  $Q$  on  $\mathcal{H}$  in a way complying the conditions in Lemma 1 and Lemma 7. Then for all classifiers with parameters satisfying  $|\tilde{\beta} - \beta| \leq \frac{\tilde{\beta}}{L}$ , where  $\tilde{\beta} = \left(\prod_{l=1}^L \|\tilde{W}_l\|_2\right)^{1/L}$ , we can derive a generalization bound by applying Theorem 2 and Lemma 1. In the second step, we investigate the number of  $\beta$  we need to cover all possible relevant classifier parameters and apply a union bound to get the final bound. The second step is essentially the same as Neyshabur et al. [30] while the first step differs by the need of incorporating Lemma 1.

We first show the first step. Given a choice of  $\beta$  independent of the training data, let

$$\sigma = \min\left(\frac{(\gamma/8\epsilon_m)^{1/L}}{\sqrt{2b(\lambda N_0^{-\alpha} + \ln 2bL)}}, \frac{\gamma}{84LB_m\beta^{L-1}\sqrt{b \ln(4bL)}}\right).$$

Assume the “prior”  $P$  on  $\mathcal{H}$  is defined by sampling the vectorized MLP parameters from  $\mathcal{N}(0, \sigma^2 I)$ ; and the “posterior”  $Q$  on  $\mathcal{H}$  is defined by first sampling a set of random perturbations  $\{U_l\}_{l=1}^L$  with  $\text{vec}(\{U_l\}_{l=1}^L) \sim \mathcal{N}(0, \sigma^2 I)$  and then adding them to  $\{\tilde{W}_l\}_{l=1}^L$ , the parameters of  $\tilde{h}$ . Then for any  $\tilde{h}$  with  $\{\tilde{W}_l\}_{l=1}^L$  satisfying  $|\tilde{\beta} - \beta| \leq \frac{\tilde{\beta}}{L}$ , by Lemma 7, we have

$$\Pr_{h \sim Q}\left(\max_{i \in V_0 \cup V_m} |h_i(X, G) - \tilde{h}_i(X, G)|_\infty < \frac{\gamma}{8}\right) > \frac{1}{2}.$$

Therefore, by applying Theorem 2, we know the bound (4) holds for  $\tilde{h}$ , i.e., with probability at least  $1 - \delta$ ,

$$\begin{aligned} & \mathcal{L}_m^0(\tilde{h}) - \hat{\mathcal{L}}_0^\gamma(\tilde{h}) \\ & \leq \frac{1}{\lambda} \left(2(D_{\text{KL}}(Q\|P) + 1) + \ln \frac{1}{\delta} + \frac{\lambda^2}{4N_0} + D_{m,0}^{\gamma/2}(P; \lambda)\right) \\ & \leq \frac{1}{\lambda} \left(2(D_{\text{KL}}(Q\|P) + 1) + \ln \frac{1}{\delta} + \frac{\lambda^2}{4N_0} + \ln 3 + \lambda cK\epsilon_m\right) \end{aligned} \quad (17)$$

$$\leq \frac{2}{N_0^{2\alpha}} D_{\text{KL}}(Q\|P) + \frac{1}{N_0^{2\alpha}} \left(\ln \frac{3}{\delta} + 2\right) + \frac{1}{4N_0^{1-2\alpha}} + cK\epsilon_m, \quad (18)$$

where in (17) we have applied Lemma 1 to bound  $D_{m,0}^{\gamma/2}(P; \lambda)$  under Assumptions 1, 2, and 3; and in (18) we have set  $\lambda = N_0^{2\alpha}$ .

Moreover, since both  $P$  and  $Q$  are normal distributions, we know that

$$D_{\text{KL}}(Q\|P) \leq \frac{\sum_{l=1}^L \|\tilde{W}_l\|_F^2}{2\sigma^2}.$$

By Assumption 4, both  $B_m$  and  $C$  are constant with respect to  $N_0$ . Later we will show that we only need  $\beta \leq C$ . Therefore, for large enough  $N_0$ , we can have

$$\frac{(\gamma/8\epsilon_m)^{1/L}}{\sqrt{2b(N_0^\alpha + \ln 2bL)}} < \frac{\gamma}{84LB_m\beta^{L-1}\sqrt{b \ln(4bL)}},$$

which implies,

$$\sigma = \frac{(\gamma/8\epsilon_m)^{1/L}}{\sqrt{2b(N_0^\alpha + \ln 2bL)}},$$

and hence,

$$D_{\text{KL}}(Q\|P) \leq \frac{b(N_0^\alpha + \ln 2bL) \sum_{l=1}^L \|\widetilde{W}_l\|_F^2}{(\gamma/8)^{2/L}} (\epsilon_m)^{2/L}. \quad (19)$$

Therefore, with probability at least  $1 - \delta$ ,

$$\begin{aligned} & \mathcal{L}_m^0(\tilde{h}) - \widehat{\mathcal{L}}_0^\gamma(\tilde{h}) \\ & \leq cK\epsilon_m + \frac{2}{N_0^{2\alpha}} D_{\text{KL}}(Q\|P) + \frac{1}{N_0^{2\alpha}} \left( \ln \frac{3}{\delta} + 2 \right) + \frac{1}{4N_0^{1-2\alpha}} \\ & \leq O \left( cK\epsilon_m + \frac{b \sum_{l=1}^L \|\widetilde{W}_l\|_F^2}{(\gamma/8)^{2/L} N_0^\alpha} (\epsilon_m)^{2/L} + \frac{1}{N_0^{1-2\alpha}} + \frac{1}{N_0^{2\alpha}} \ln \frac{1}{\delta} \right). \end{aligned} \quad (20)$$

Then we show the second step, i.e., finding out the number of  $\beta$  we need to cover all possible relevant classifier parameters. Similarly as Neyshabur et al. [30], we will show that we only need to consider  $(\frac{\gamma}{2B_m})^{1/L} \leq \tilde{\beta} \leq C$  (recall that  $\|\widetilde{W}_l\|_F \leq C, l = 1, \dots, L$ ). For any  $\tilde{\beta}$  outside this range, the bound (16) automatically holds. If  $\tilde{\beta} < (\frac{\gamma}{2B_m})^{1/L}$ , then for any node  $i \in V_0$ ,  $\|\tilde{h}_i(X, G)\|_\infty < \frac{\gamma}{2}$ , which implies  $\widehat{\mathcal{L}}_0^\gamma(\tilde{h}) = 1$  as the difference between any two output logits for any training node is smaller than  $\gamma$ . Also noticing that  $\mathcal{L}_m^0(\tilde{h}) \leq 1$  by definition, so the bound (16) trivially holds. And for  $\tilde{\beta}$  in this range,  $|\beta - \tilde{\beta}| \leq \frac{1}{L} (\frac{\gamma}{2B_m})^{1/L}$  is a sufficient condition for  $\beta$  to satisfy  $|\tilde{\beta} - \beta| \leq \frac{\tilde{\beta}}{L}$ , and we need at most  $\frac{LC(2B_m)^{1/L}}{\gamma^{1/L}}$  of  $\beta$  to cover all  $\tilde{\beta}$  in the above range. Taking a union bound on all such  $\beta$ , which is equivalent to replace  $\delta$  with  $\frac{\delta}{\frac{LC(2B_m)^{1/L}}{\gamma^{1/L}}}$  in (20), it gives us the final result: with probability at least  $1 - \delta$ ,

$$\mathcal{L}_m^0(\tilde{h}) - \widehat{\mathcal{L}}_0^\gamma(\tilde{h}) \leq O \left( cK\epsilon_m + \frac{b \sum_{l=1}^L \|\widetilde{W}_l\|_F^2}{(\gamma/8)^{2/L} N_0^\alpha} (\epsilon_m)^{2/L} + \frac{1}{N_0^{1-2\alpha}} + \frac{1}{N_0^{2\alpha}} \ln \frac{LC(2B_m)^{1/L}}{\gamma^{1/L} \delta} \right).$$

□

### A.5 Discussion on Assumption 3

To better understand Assumption 3, we show a simplified scenario where this assumption holds.

We discuss in the context where the classification problem has binary labels and the MLP of the classifier  $h$  only consists of a linear layer with parameters  $W \in \mathbb{R}^{D' \times 2}$ . In this case, the distribution  $P$  on  $\mathcal{H}$  in Assumption 3 is defined by sampling the vectorized parameters  $\text{vec}(W) \sim \mathcal{N}(0, \sigma^2 I_{2D'})$ . Under Assumption 2, each training sample in  $V_0$  has a near set in  $V_m$  with the same size  $s_m$ . For simplicity, we consider the case where  $s_m = 1$ . Let  $Z^{(0)}, Z^{(m)} \in \mathbb{R}^{N_0 \times D'}$  be the aggregated node features of  $V_0$  and  $V_m$  respectively. Without loss of generality, assume for each  $i = 1, \dots, N_0$ , the closest point in  $Z^{(0)}$  for  $Z_i^{(m)}$  is  $Z_i^{(0)}$ . To simplify the notations, we define  $Z := Z^{(0)}$  and  $\varepsilon := Z^{(m)} - Z^{(0)}$ . We always treat  $M_i$  for any matrix  $M$  as the transpose of the  $i$ -th row of  $M$  and define  $M_{(i)}$  as the  $i$ -th column vector of  $M$ .

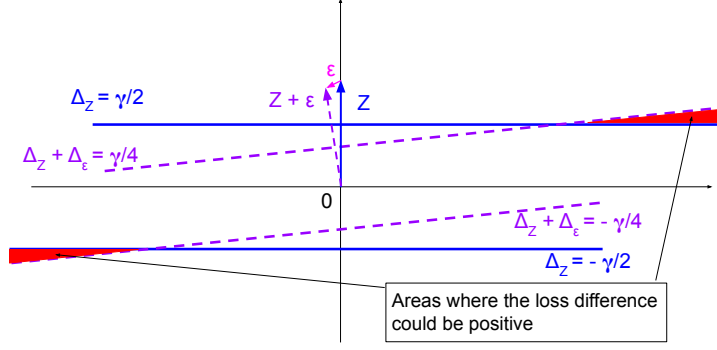


Figure 6: An illustrative example of areas in the space of  $\Delta_W$  where the loss difference term for an index  $i$  could be positive. For visual simplicity in the figure, we have used  $Z$  and  $\varepsilon$  to represent  $Z_i$  and  $\varepsilon_i$ .

Following the proof of Lemma 5, and in particular, Eq. (13), it is easy to show that, for any  $h \in \mathcal{H}$  with parameters  $W$ ,

$$\begin{aligned}
& \mathcal{L}_m^{\gamma/4}(h) - \mathcal{L}_0^{\gamma/2}(h) \\
& \leq \frac{1}{N_0} \sum_{i=1}^{N_0} \sum_{k=1}^2 \eta_k(Z_i^{(m)}) \left( \mathcal{L}^{\gamma/4}((Z^{(m)} \cdot W)_{i,k}) - \mathcal{L}^{\gamma/2}((Z^{(0)} \cdot W)_{i,k}) \right) + c\epsilon_m \\
& = 2c\epsilon_m + \frac{1}{N_0} \sum_{i=1}^{N_0} \sum_{k=1}^2 \eta_k(Z_i^{(m)}) \left( \mathbb{1} \left[ W_{(k)}^T(Z_i + \varepsilon_i) < \frac{\gamma}{4} + W_{(3-k)}^T(Z_i + \varepsilon_i) \right] - \mathbb{1} \left[ W_{(k)}^T Z_i < \frac{\gamma}{2} + W_{(3-k)}^T Z_i \right] \right). \tag{21}
\end{aligned}$$

For Assumption 3 to hold, a sufficient condition is to have the second term in Eq. (21) smaller than  $N^\alpha$  for any  $h$ . Below we will investigate when this sufficient condition holds.

To further simplify the notations, we define  $\Delta_W := W_{(1)} - W_{(2)}$ ,  $\Delta_Z := Z\Delta_W$ ,  $\Delta_\varepsilon := \varepsilon\Delta_W$ , and  $\eta_k^i := \eta_k(Z_i^{(m)})$ . Then

$$\begin{aligned}
& \mathcal{L}_m^{\gamma/4}(h) - \mathcal{L}_0^{\gamma/2}(h) \\
& \leq 2c\epsilon_m + \frac{1}{N_0} \sum_{i=1}^{N_0} \sum_{k=1}^2 \eta_k^i \left( \mathbb{1} \left[ (-1)^{k+1}(\Delta_Z + \Delta_\varepsilon)_i < \frac{\gamma}{4} \right] - \mathbb{1} \left[ (-1)^{k+1}\Delta_{Zi} < \frac{\gamma}{2} \right] \right). \tag{22}
\end{aligned}$$

Note that since  $\text{vec}(W) \sim \mathcal{N}(0, \sigma^2 I_{2D'})$ , we have  $\Delta_W \sim \mathcal{N}(0, 2\sigma^2 I_{D'})$ . And the second term in (22) depends on  $W$  only through  $\Delta_W$ .

Table 1: Possible values of the loss difference term for each index  $i = 1, \dots, N_0$ .

	$\Delta_{Zi} > \frac{\gamma}{2}$	$\Delta_{Zi} < -\frac{\gamma}{2}$	$-\frac{\gamma}{2} \leq \Delta_{Zi} \leq \frac{\gamma}{2}$
$(\Delta_Z + \Delta_\varepsilon)_i > \frac{\gamma}{4}$	0	$\eta_2^i - \eta_1^i$	$-\eta_1^i$
$(\Delta_Z + \Delta_\varepsilon)_i < -\frac{\gamma}{4}$	$\eta_1^i - \eta_2^i$	0	$-\eta_2^i$
$-\frac{\gamma}{4} \leq (\Delta_Z + \Delta_\varepsilon)_i \leq \frac{\gamma}{4}$	$\eta_1^i$	$\eta_2^i$	0

For each  $i = 1, \dots, N_0$ , the term  $\sum_{k=1}^2 \eta_k^i \left( \mathbb{1} \left[ (-1)^{k+1}(\Delta_Z + \Delta_\varepsilon)_i < \frac{\gamma}{4} \right] - \mathbb{1} \left[ (-1)^{k+1}\Delta_{Zi} < \frac{\gamma}{2} \right] \right)$  in (22) has only a few possible values, which can be summarized in the following 9 cases in Table 1. As can be seen, this loss difference term could be positive only when (1)  $\Delta_{Zi} > \frac{\gamma}{2}$  and  $(\Delta_Z + \Delta_\varepsilon)_i \leq \frac{\gamma}{4}$  or (2)  $\Delta_{Zi} < -\frac{\gamma}{2}$  and  $(\Delta_Z + \Delta_\varepsilon)_i \geq -\frac{\gamma}{4}$ . This implies that, for fixed  $Z_i$  and  $\varepsilon_i$ , there are two linear subspaces in the space of  $\Delta_W$  where the loss difference for index  $i$  could be positive. In Figure 6, we provide an illustrative example of such linear subspaces in the case  $\Delta_W \in \mathbb{R}^2$ , such that we can visualize it. Qualitatively, when  $\|\varepsilon_i\|_2$  is much smaller than  $\|Z_i\|_2$  (which is often the case by their constructions), the areas that the loss difference term being positive will be very small.



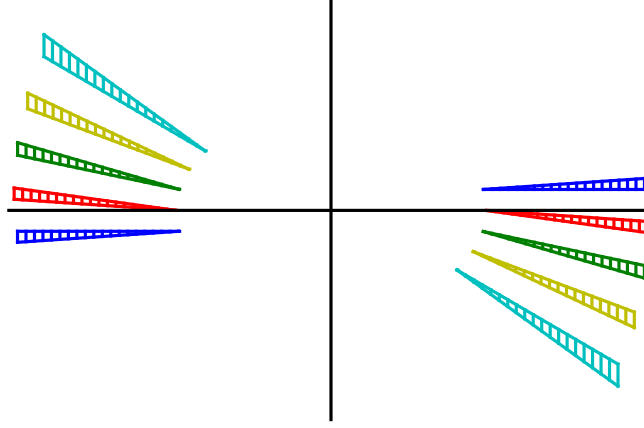


Figure 7: An illustrative example of data points with no intersected positive areas. Only the positive areas as shown in Figure 6 are visualized. Each color corresponds to a unique index  $i$ . As shown in the figure, there are no intersections among the areas of different data points when the  $Z_i$ 's are nicely scattered and  $\varepsilon_i$ 's are small.

For a classifier  $h$  to have  $\mathcal{L}_m^{\gamma/4}(h) - \mathcal{L}_0^{\gamma/2}(h) > cK\epsilon_m + N_0^{-\alpha}$ , a necessary condition is that its corresponding  $\Delta_W$  lies in the intersection of positive areas of at least  $N_0^{1-\alpha}$  samples. Conversely, if  $\varepsilon_i$ 's are small and  $Z_i$ 's are nicely scattered such that the  $N_0$  samples can be divided into  $N_0^\alpha$  groups where the positive areas of any two points from different groups do not intersect, then we know  $\mathcal{L}_m^{\gamma/4}(h) - \mathcal{L}_0^{\gamma/2}(h) \leq cK\epsilon_m + N_0^{-\alpha}$  for any  $h$ . And hence this is a sufficient condition for Assumption 3 to hold. Figure 7 provides an illustrative example of data points with no intersected positive areas on a 2-dimensional surface. When  $D' > 2$ , it might be difficult to completely avoid intersections of the positive areas. However, what Assumption 3 requires is that the areas where a large number of data points intersect are small.

## B More Details of Experiment Setup

In this section, we describe more details of our experiment setup that are omitted in the main paper due to the space limit.

### B.1 Detailed Training Setup

We use the default setting in Deep Graph Library [43]<sup>12</sup> for model hyper-parameters. We use the Adam optimizer with an initial learning rate of 0.01 and weight decay of 5e-4 to train all models for 400 epochs by minimizing the cross-entropy loss, with early stopping on the validation set.

### B.2 Detailed Setup of the Noisy Feature Experiment

In this experiment (corresponding to Figure 4), we make the node features less homophilous by adding random noises to each node independently. Specifically, we use noisy features  $\tilde{X} = X + \alpha \frac{\|X\|_F}{\|U\|_F} U$ , where  $X \in \mathbb{R}^{N \times D}$  is the original feature matrix, and  $U \in \mathbb{R}^{N \times D}$  is a random matrix with each element independently and uniformly sampled from  $[0, 1]$ . And we set  $\alpha = 5$ . In this way, the magnitude of the noise is slightly larger than the original feature to significantly reduce the homophily property. All other experiment settings are the same as those corresponding to Figure 1.

<sup>12</sup>Apache License 2.0.

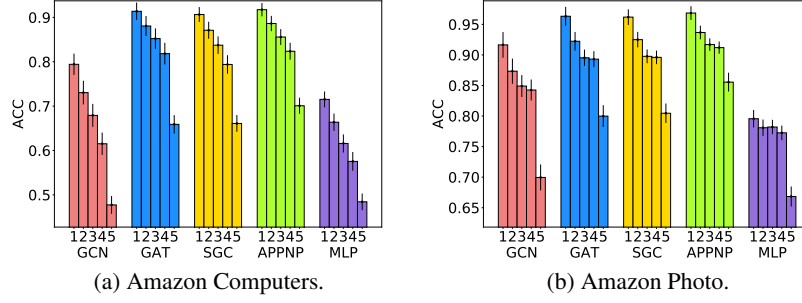


Figure 8: Test accuracy disparity across subgroups by aggregated-feature distance. Extra experiments on Amazon-Computers and Amazon-Photo datasets. The experiment and plot settings are the same as Figure 1.

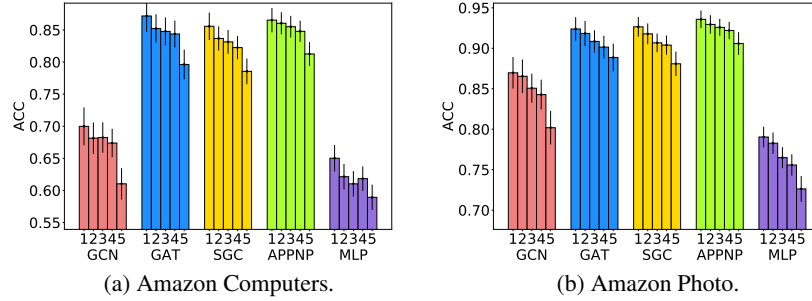


Figure 9: Test accuracy disparity across subgroups by geodesic distance. Extra experiments on Amazon-Computers and Amazon-Photo datasets. The experiment and plot settings are the same as Figure 2.

### B.3 Detailed Setup of the Biased Training Node Selection Experiment

In this experiment (corresponding to Section 5.2), we investigate the impact of biased training node selection. As briefly described in Section 5.2, we choose a “dominant class” and construct a manipulated training set. For each class, we still sample 20 training nodes but in a biased way. Specifically, given one choice of the four node centrality metrics (degree, closeness, betweenness, and PageRank), the training set is sampled as follows.

1. For the dominant class, uniformly sample 15 nodes from the 10% of the nodes with highest node centrality, and uniformly sample 5 nodes from the remaining.
2. For each of the other classes, uniformly sample 15 nodes from the 10% of the nodes with lowest node centrality, and uniformly sample 5 nodes from the remaining.

In this way, the training nodes of the dominant class are biased towards high-centrality nodes while the training nodes of the other classes are biased towards low-centrality nodes.

After the biased training set is constructed, we randomly sample 500 validation nodes and 1000 test nodes from the remaining nodes and perform the model training following the standard setup as the previous experiments.

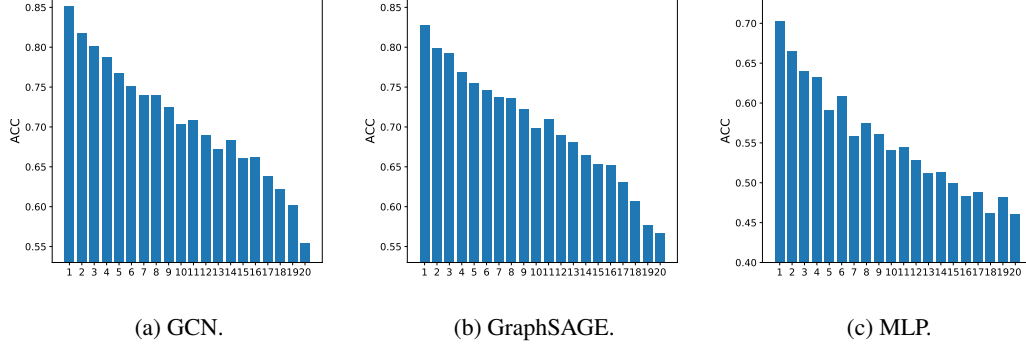


Figure 10: Results on OGBN-Arxiv. Test accuracy disparity across subgroups by aggregated-feature distance. Each figure corresponds to a model. Bars labeled 1 to 20 represent subgroups with increasing distance to training set.

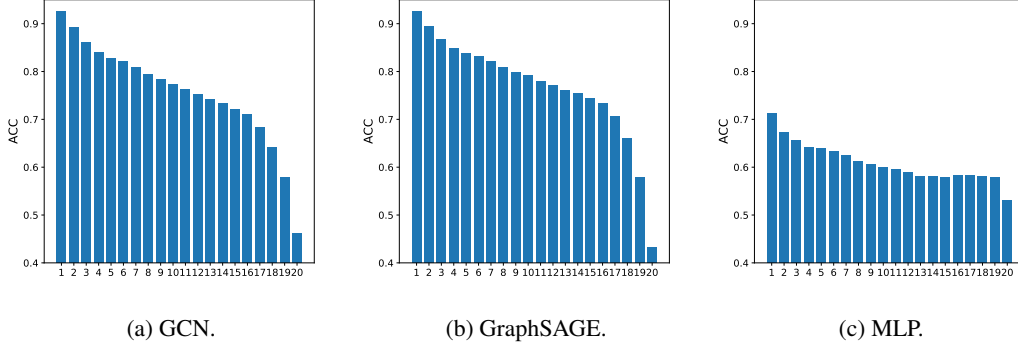


Figure 11: Results on OGBN-Products. Test accuracy disparity across subgroups by aggregated-feature distance. The experiment and plot settings are the same as Figure 10.

## C Extra Experiment Results

### C.1 Accuracy Disparity on Amazon Datasets

In addition to the commonly used citation network benchmarks, Cora, Citeseer, and Pubmed [37, 47], we also provide results of the test accuracy disparity experiments of subgroups by aggregated-feature distance and geodesic distance on Amazon-Computers and Amazon-Photo datasets [38], which have a similar scale but a different network type compared to the three citation networks.

For Amazon-Computers and Amazon-Photo, we follow exactly the same experiment procedure as for Cora, Citeseer, and Pubmed. The results of subgroups by aggregated-feature distance are shown in Figure 8 and the results of subgroups by geodesic distance are shown in Figure 9. The results are respectively similar as those in Figure 1 and Figure 2.

### C.2 Accuracy Disparity on Open Graph Benchmarks

We further provide experiment results on two large-scale datasets from Open Graph Benchmark [17], OGBN-Arxiv and OGBN-Products.

For OGBN-Arxiv and OGBN-Products, we first follow the standard training procedure suggested by Open Graph Benchmark [17] to train a GCN, a GraphSAGE, and an MLP. And we split the test groups into 20 groups in terms of the aggregated feature distance. As there are more test nodes available, we can afford the split of more groups better resolution. The results on OGBN-Arxiv and OGBN-

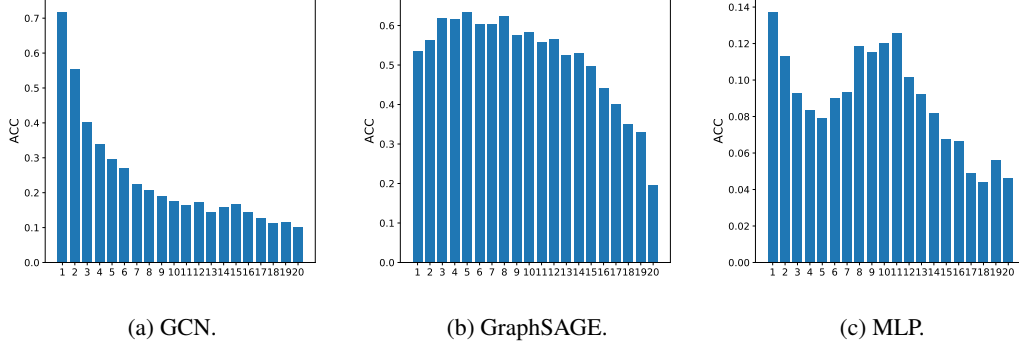


Figure 12: Results on OGBN-Arxiv. Test accuracy disparity across subgroups by aggregated-feature distance, experimented with noisy features. The experiment and plot settings are the same as Figure 10, except the node features are perturbed by independent noises to reduce homophily.

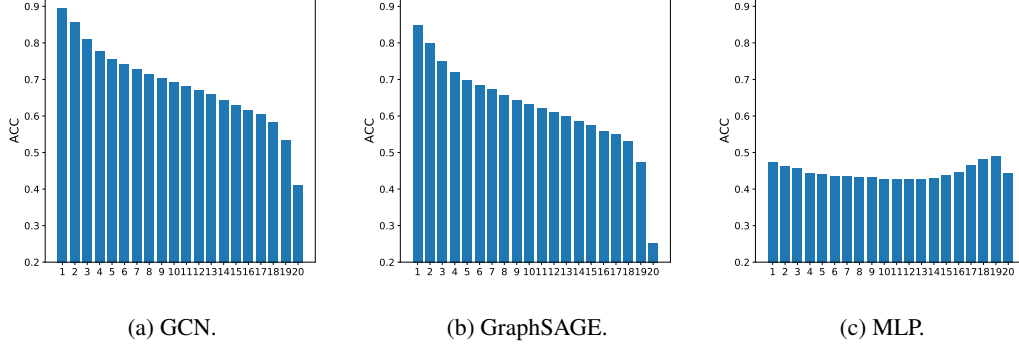


Figure 13: Results on OGBN-Products. Test accuracy disparity across subgroups by aggregated-feature distance, experimented with noisy features. The experiment and plot settings are the same as Figure 11, except for the node features are perturbed by independent noises to reduce homophily.

Products are respectively shown in Figure 10 and Figure 11, where we observe a similar decreasing pattern of test accuracy as in Figure 1 (on the citation networks). Since there is also a decreasing pattern for MLP, following the experiments shown in Figure 4, we further inject independent noises to node features to reduce the homophily of the OGBN-Arxiv and OGBN-Products dataset and repeat the experiments in Figure 10 and Figure 11. The results are respectively shown in Figure 12 and Figure 13, where, similar as Figure 4, the decreasing pattern largely remains for GNNs but disappears for the MLP.

We also experiment on subgroups split in terms of geodesic distance and node centrality metrics. The results of these experiments are slightly different on the large-scale datasets compared to those on the smaller benchmark datasets.

For geodesic distance (Figure 14 for OGBN-Arxiv and Figure 15 for OGBN-Products), there is not a descending trend of test accuracy until the last few groups. This is because the size of training set is large such that most test nodes are 1-hop neighbors of some training nodes. Therefore most groups are random split of such 1-hop neighbors and there will not be a descending accuracy among these subgroups. This problem is especially obvious for OGBN-Arxiv, where 60% of the nodes are in the training set. So we only see an accuracy drop on the last two subgroups. The size of training set is relatively smaller on OGBN-Products but still more than 60% of the test nodes are 1-hop neighbors of some training nodes. It is worth-noting that the plots in Figure 15 have stair patterns, showing a clear descending trend with respect to the geodesic distance. The fluctuation of early subgroups is larger on

OGBN-Arxiv because there are fewer test nodes in OGBN-Arxiv than in OGBN-Products. Overall, there is still a clear descending trend with respect to increasing geodesic distance. But the nodes are less distinguishable in terms of geodesic distance than aggregated-feature distance, especially when the size of training set is large (more discussions in Appendix D.1).

For node centrality metrics, we report experiments on degree and PageRank, and omit the betweenness and closeness metrics due to their high computation cost on large-scale graphs. The results on OGBN-Arxiv are shown in Figure 16. It is intriguing that there is a descending trend with respect to the degree and PageRank metrics on this particular experiment setting, though the descending trend is not as sharp as the one in Figure 10 (experiments on aggregated-feature distance). It is possible that, when there is a very large training set (60% in this case), the node centrality metrics become related to the aggregated-feature distance. However, node centrality metrics again fail to capture the descending trend on OGBN-Products, as shown in Figure 17. In future work, we plan to further explore the relationship between the theoretically derived aggregated-feature distance and various more intuitive graph metrics on different graph data.

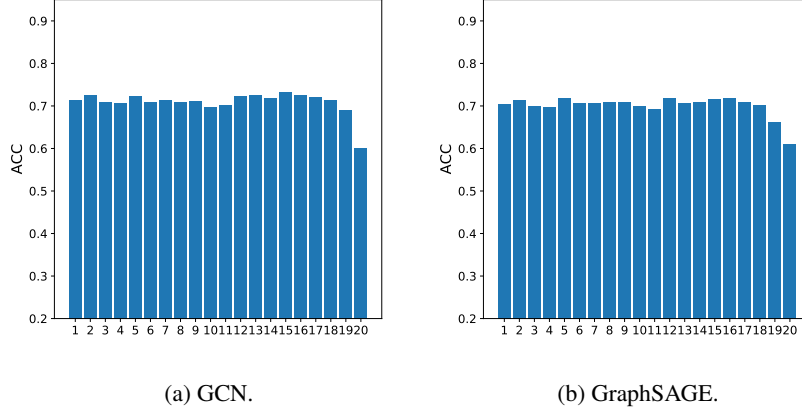


Figure 14: Results on OGBN-Arxiv. Test accuracy disparity across subgroups by geodesic distance. The experiment and plot settings are the same as Figure 10, except for the aggregated-feature distance is replaced by the geodesic distance.

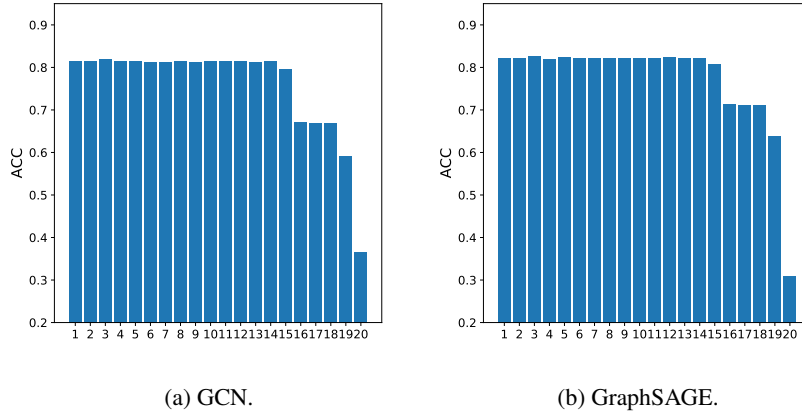
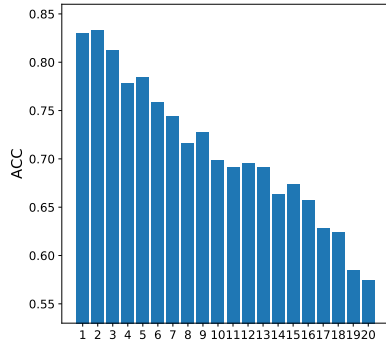
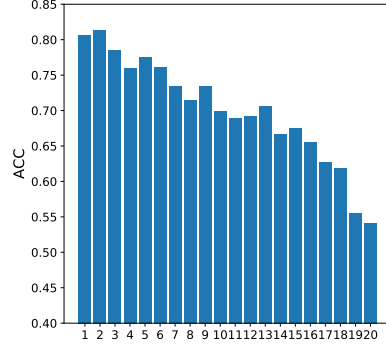


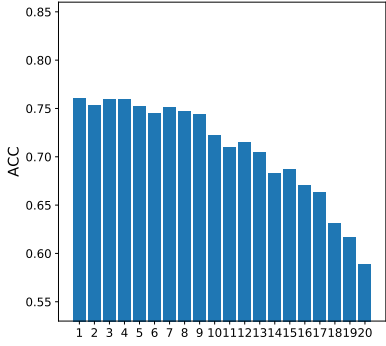
Figure 15: Results on OGBN-Products. Test accuracy disparity across subgroups by geodesic distance. The experiment and plot settings are the same as Figure 14.



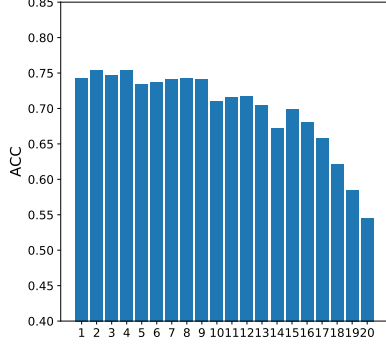
(a) GCN. Subgroup by degree.



(b) GraphSAGE. Subgroup by degree.



(c) GCN. Subgroup by PageRank.



(d) GraphSAGE. Subgroup by PageRank.

Figure 16: Results on OGBN-Arxiv. Test accuracy disparity across subgroups by node centrality metrics. The experiment and plot settings are the same as Figure 10.

### C.3 More Results of Biased Training Node Selection

In Figure 5 of Section 5.2, we have shown that the learned GNN models will be biased towards the labels of training nodes of higher centrality (while the learned MLP models do not show a similar trend). Due to the space limit, in the main paper, we are only able to report the experiment results on Cora with a particular class selected as the “dominant” class. Here we report the full experiment results on three datasets, with each class selected as the “dominant” class. The results on Cora, Citeseer, and Pubmed are respectively shown in Figures 18, 19, and 20. As can be seen from the figures, the observed phenomenon is consistent over almost all settings.

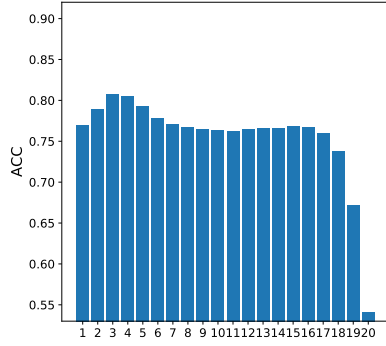
## D Discussions

### D.1 Relationship Between Aggregated-Feature Distance and Geodesic Distance

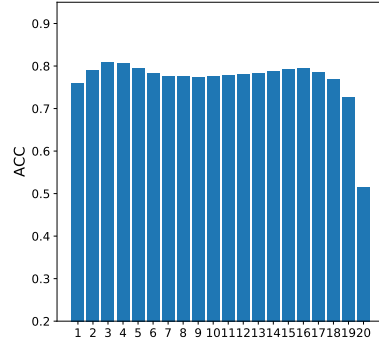
We discuss two scenarios where the aggregated-feature distance and the geodesic distance are likely to be related.

*Smoothing effect of feature aggregation in GNNs.* Many existing GNN models are known to have a smoothing effect on the aggregated node features [24]. As a result, nodes with a shorter geodesic distance are likely to have more similar aggregated features.

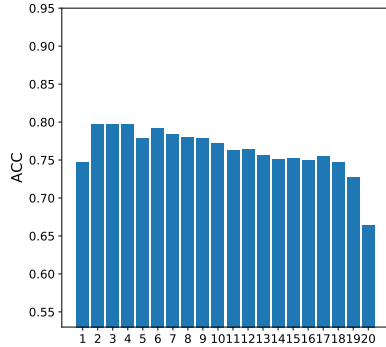
*Homophily.* Many real-world graph-structured data exhibit a homophily property [28], i.e., connected nodes tend to share similar attributes. In this case, again, nodes with a shorter geodesic distance on the graph tend to have more similar aggregated features.



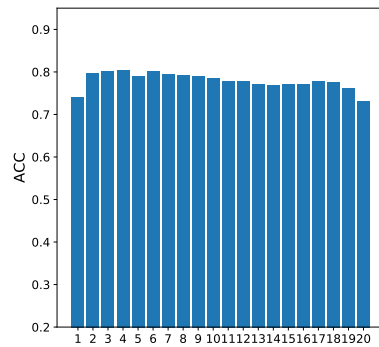
(a) GCN. Subgroup by degree.



(b) GraphSAGE. Subgroup by degree.



(c) GCN. Subgroup by PageRank.



(d) GraphSAGE. Subgroup by PageRank.

Figure 17: Results on OGBN-Products. Test accuracy disparity across subgroups by node centrality metrics. The experiment and plot settings are the same as Figure 11.

However, the geodesic distance is usually coarser-grained than the aggregated-feature distance due to its discrete nature. When the graph is a “small world” [44] and the number of training nodes is large, the geodesic distance from most test nodes to the set of training nodes will concentrate on 1 or 2 hops, making the test nodes indistinguishable with respect to this metric.

It is an interesting future direction to explore interpretable graph metrics that may better relate to the aggregated-feature distance.

## D.2 Implications for GNN Generalization under Non-Homophily

A number of recent studies suggest that classical GNNs (e.g., GCN [20]) can only work well when the labels of connected nodes are similar [31, 16, 52], which is now commonly referred as homophily [28]. However, homophily is not a necessary condition to have small generalization errors in our analysis. Instead, good generalization can be achieved when the aggregated features of test nodes are close to those of some training nodes. Interestingly, a concurrent work [26] of this paper observes a similar phenomenon with empirical evidence.

The new results by Ma et al. [26] and our work suggest that the space of non-homophilous data can be further dissected into more fine-grained categories, which may motivate designs of new GNN models tailored for each category.

### D.3 Limitations of the Analysis

To our best knowledge, this work is one of the first attempts<sup>13</sup> to theoretically analyze the generalization ability of GNNs under non-IID node-level semi-supervised learning tasks. While we believe this work presents non-trivial contributions towards the theoretical understanding of generalization and fairness of GNNs with supportive empirical evidence, there are a few limitations of the current analysis which we hope to improve in future work.

The first limitation is that the derived generalization bounds do not yet match the practical performances of GNNs. This limitation is partly inherited from the mismatch between the theories and the practices of deep learning in general, as we utilize the results by Neyshabur et al. [30] to illustrate the characteristics of the neural-network part of GNNs. In future work, we hope to adapt stronger PAC-Bayesian bounds for neural networks under IID setup [51, 10] to the non-IID setup for GNNs.

Another limitation is that we have assumed a particular form of GNNs similar as SGC [45] or APPNP [21]. This form of GNNs simplifies the analysis but does not include some common GNNs such as GCN [20] and GAT [41]. We notice that the key characteristics of GNNs we need for the analysis are that the change of outputs of GNNs under certain perturbations needs to be bounded. A recent work [25] has shown that some more general forms of GNNs (including GCN) indeed have bounded output changes under perturbations. So the analysis in this work can be potentially adapted to more general forms of GNNs by utilizing such perturbation bounds. Empirically, we have demonstrated that the accuracy disparity phenomenon predicted by our theoretical analysis indeed appears in experiments on GCN, GAT, and GraphSAGE.

Finally, our analysis requires some assumptions on the relationship between the training set and the target test subgroup. While, not surprisingly, we have to make some assumptions about this relationship to expect good generalization to the target subgroup, it is an interesting future direction to explore more relaxed assumptions than the ones used in this work.

### D.4 Societal Impacts

As GNNs have been deployed in human-related real-world applications such as recommender systems [48], understanding the fairness issues of GNNs may have direct societal impacts. On the positive side, understanding the systematic biases embedded in the GNN models and the graph-structured data helps researchers and practitioners come up with solutions that mitigate the potential harms resulted by such biases. On the negative side, however, such understanding may also be used for malicious purposes: e.g., performing adversarial attacks on GNNs that utilizes systematic biases. Nevertheless, we believe the theoretical understandings resulting from this work contribute to a small step towards making the GNN models more transparent to the research community, which may motivate the design of better and fairer models.

---

<sup>13</sup>The only other work we are aware of is by Baranwal et al. [3], where strong assumptions (CSBM) on the data generating mechanisms are made.



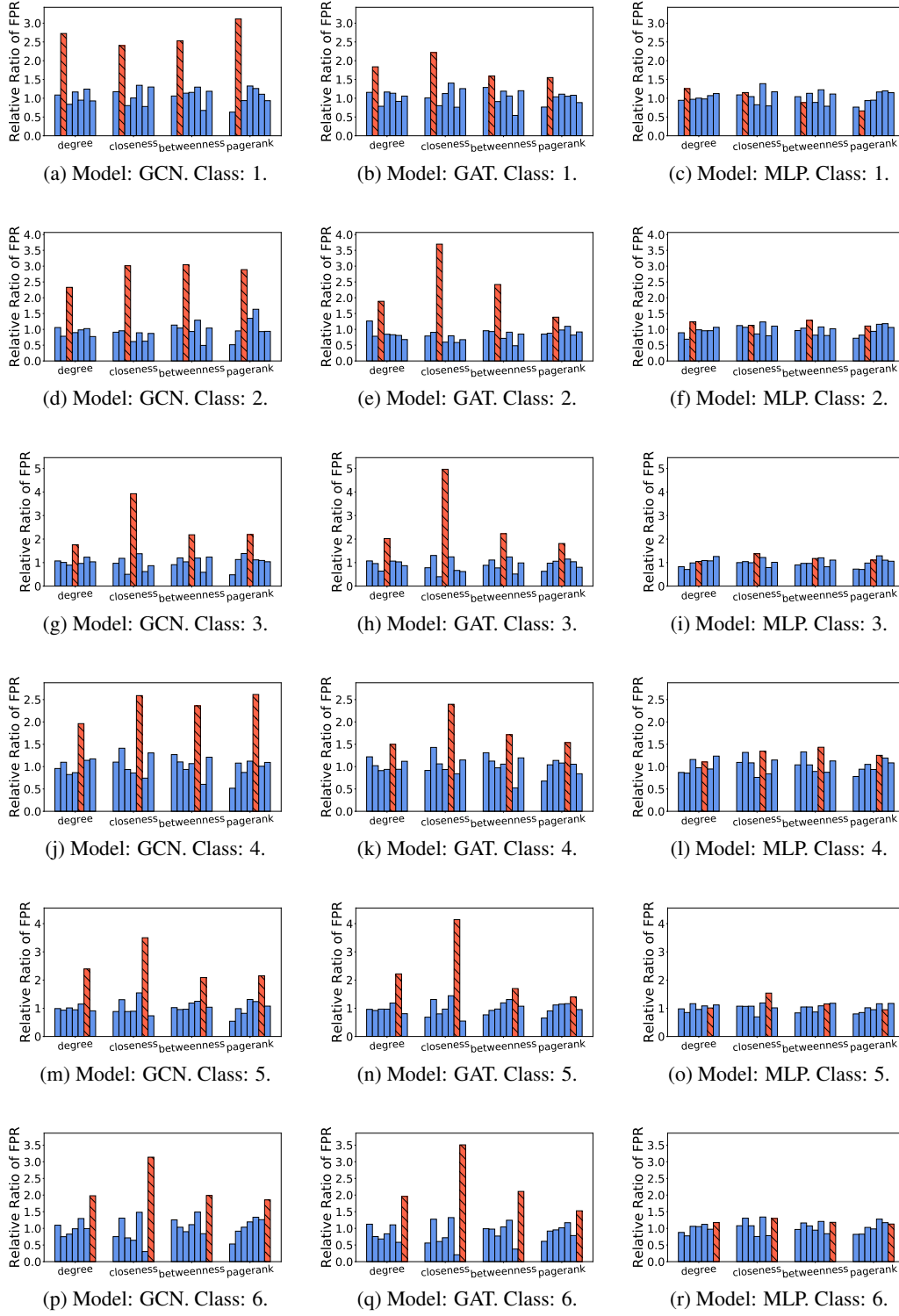


Figure 18: Relative ratio of FPR in the biased training node selection experiment. Remaining results on Cora besides Figure 5. Each row corresponds to a different dominant class of choice. See Figure 5 for the plot settings.

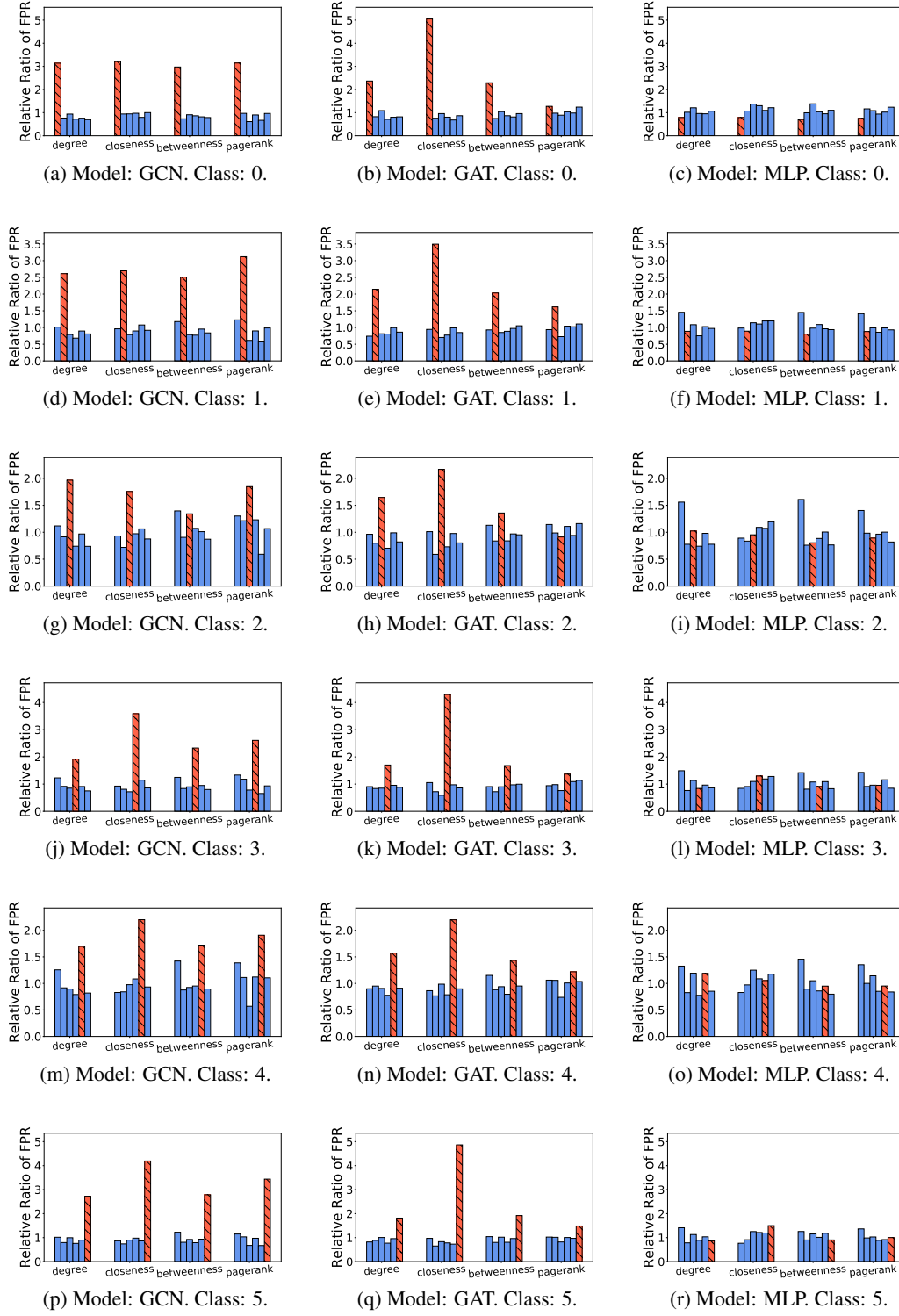


Figure 19: Relative ratio of FPR in the biased training node selection experiment. Full results on Citeseer. Each row corresponds to a different dominant class of choice. See Figure 5 for the plot settings.

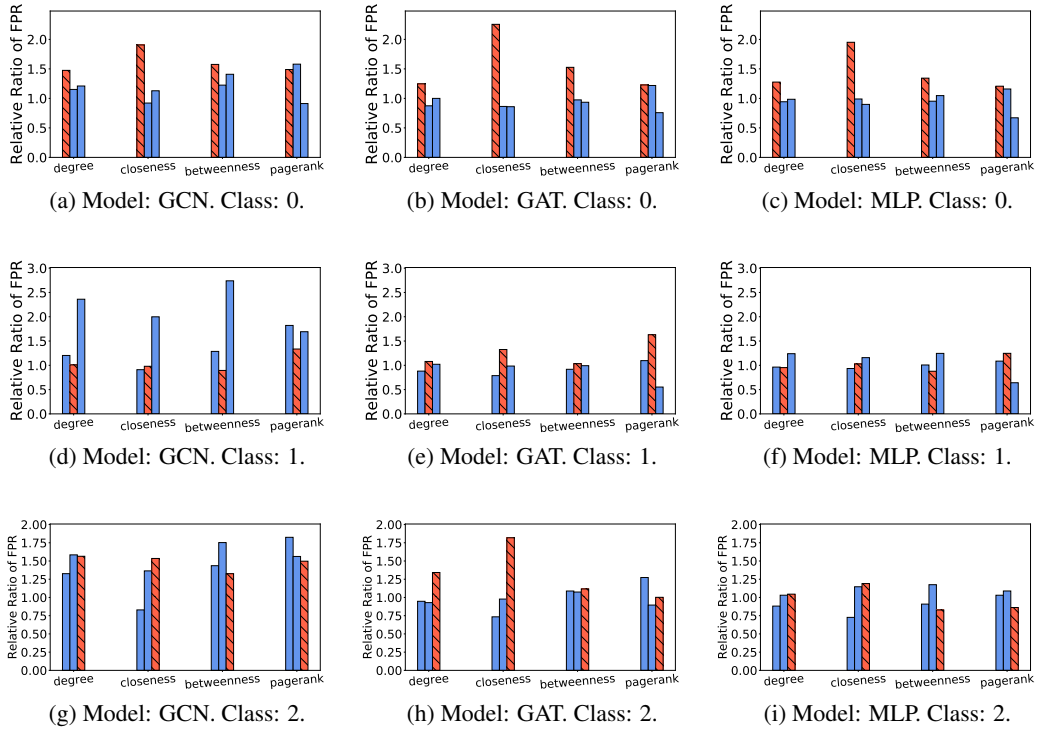


Figure 20: Relative ratio of FPR in the biased training node selection experiment. Full results on Pubmed. Each row corresponds to a different dominant class of choice. See Figure 5 for the plot settings.